PHILOSOPHICAL TRANSACTIONS OF THE ROYAL SOCIETY A MATHEMATICAL, PHYSICAL & ENGINEERING SCIENCES

Theoretical and Numerical Structure of Unstable Detonations

Anne Bourlioux and Andrew J. Majda

Phil. Trans. R. Soc. Lond. A 1995 **350**, 29-68
doi: 10.1098/rsta.1995.0002

Theoretical and numerical structure of unstable detonations

By Anne Bourlioux[1] and Andrew J. Majda[2]

[1]*Department of Mathematics, University of California, Berkeley, California 094720, U.S.A.*

[2]*Program in Applied and Computational Mathematics and Department of Mathematics, Princeton University, Princeton, New Jersey 08544, U.S.A.*

Contents

PAGE

1. Introduction 30
2. Basic theory of ZND waves 30
   (*a*) Basic equations 31
   (*b*) ZND waves 31
   (*c*) A qualitative–quantitative asymptotic model for detonation waves 32
3. Stable and unstable ZND waves in one dimension 34
   (*a*) Linearized stability of ZND waves in one dimension 34
   (*b*) Numerical computation of stable ZND waves 36
   (*c*) Numerical computation of unstable ZND waves 37
   (*d*) Asymptotic theory for detonation instability in one dimension 40
   (*e*) Interaction of asymptotic theory and numerics in predicting one-dimensional detonation instability 42
4. Theories for detonation instability in multi-dimensions 44
   (*a*) Linearized instability of ZND waves in multi-dimensions 44
   (*b*) Geometric acoustics and detonation instability 47
   (*c*) Theoretical predictions for cell spacing via detonation instability 48
   (*d*) Low-frequency asymptotic theories for pattern formation in unstable detonations 49
5. Numerical and theoretical structure for two-dimensional unstable detonations 54
   (*a*) A new numerical method for unstable detonations 54
   (*b*) Recent insight into the physical phenomena of unstable detonations 56
   (*c*) Comparison of theory and numerics 61
6. Concluding remarks 66

References 66

In this review, we emphasize the recent progress achieved in understanding the behaviour of unstable detonations through the interaction of theoretical, asymptotic, and numerical ideas. Theoretical predictions and numerical simulations for unstable one-dimensional detonations are described in detail as an important testing ground for the more complex ideas and phenomena that occur in several space dimensions. The linear and nonlinear theories for unstable detonations are generalized to several space dimensions. A new dedicated numerical method leads

Phil. Trans. R. Soc. Lond. A (1995) **350**, 29–68
Printed in Great Britain

to better insight into the physical phenomena of unstable detonations, such as the nature of the turbulence generated in the wake of the front. Simplified models derived through asymptotics and comparisons between theoretical and numerical predictions are stressed throughout this paper.

1. Introduction

The classical theory of von Neumann, Zeldovich, and Döring postulates that detonation waves are steady travelling waves (ZND waves) with a quasi-one-dimensional structure consisting of an ordinary fluid dynamic shock followed by a reaction zone. However, experiments reveal that detonation waves are often unstable with remarkable transverse wave structures and much larger local pressures than are predicted by the classical ZND theory (Oppenheim 1972; Fickett & Davis 1979). Understanding such instabilities is important in a wide variety of contexts involving both safety and enhanced combustion. For example, in a non-traditional application involving the development of supersonic propulsion devices, the oblique detonation wave engine has been proposed as an alternative to the Scramjet concept. In the oblique detonation wave engine, the burning takes place in oblique overdriven detonations attached to wedge-like surfaces. It is obvious that the stability characteristics of overdriven detonations are important for the design process.

Two main points of view are emphasized in this review. The first point is the symbiotic interaction of asymptotics, numerics, and analysis in yielding an improved understanding of detonation instability, The second point is the use of the simplest model, which involves the inviscid compressible reacting Euler equations with an ideal gas law and irreversible Arrhenius kinetics for a single reaction progress variable. This second point is validated by the fact that a remarkable range of phenomena for unstable detonations documented in experiments occurs in the model in a qualitative fashion as we vary a few simple parameters of the basic ZND wave such as the heat release, activation energy, and overdrive.

In § 2, the model and its properties and we also sketch the derivation of a simpler asymptotic model. The material in § 3 provides a self-contained review of the recent multi-faceted study of detonation instability in the simplest context of a single space variable, while in § 4 and § 5 we discuss instabilities in two space variables. The work in § 5 includes a discussion of a new 'state of the art' numerical method designed specifically for computing detonation instability in several space dimensions. New insights into the physical mechanisms of detonation instability which have been achieved with this method are also described in § 5. A 'numerical test suite' of benchmark problems for designing numerical methods for unstable detonations is also introduced, in one space dimension (§ 3) and in two space dimensions (§ 5).

2. Basic theory of ZND waves

In this section we list the basic equations and briefly summarize the elementary properties of ZND waves which are needed in subsequent sections. We also review the asymptotic derivation of a qualitative–quantitative model for deto-

nation waves in high Mach number combustion. This simplified model provides elementary insights into the propagation of detonation waves as well as a class of extremely simple but instructive test problems for numerical methods for computing detonations (see § 3 below).

(*a*) *Basic equations*

In this review we consider solutions of the Euler equations for inviscid reacting gas flow so we neglect all dissipation mechanisms. For the chemical interaction we consider the simplest model. There are only two species present, the reactant and the product, and the reactant is converted to the product by a one-step irreversible chemical reaction governed by Arrhenius kinetics. With these simplifying assumptions the equations for reacting flow are given by

$$\left.\begin{aligned} \rho_t + \nabla\cdot(\rho\boldsymbol{v}) = 0, \quad (\rho\boldsymbol{v})_t + \nabla\cdot(\rho\boldsymbol{v}\boldsymbol{v}) + \nabla p = 0, \\ (\rho E)_t + \nabla\cdot(\rho\boldsymbol{v}E + \boldsymbol{v}p) = 0, \quad (\rho Z)_t + \nabla\cdot(\rho\boldsymbol{v}Z) = -w, \end{aligned}\right\} \tag{2.1}$$

with

$$\left.\begin{aligned} E = e + q_0 Z + \tfrac{1}{2}v^2, \quad p = (\gamma-1)\rho e, \\ T = p/\rho, \quad w = K\rho Z\exp(-E^+/T). \end{aligned}\right\} \tag{2.2}$$

In these equations, p, ρ, T, $\boldsymbol{v}$, E, respectively, the pressure, density, temperature, velocity, specific energy, and reactant mass fraction. The variables have been made dimensionless by reference to a fixed constant state. The dimensionless parameters appearing above are the specific heat ratio, γ, the heat release parameter, q_0, and the activation energy, E^+.

(*b*) *ZND waves*

The equations in (2.1) have explicit travelling wave profiles consisting of a precursor ordinary fluid dynamics shock followed by a chemical reaction. These profiles are the ZND waves and are readily computed by quadrature of a single nonlinear ordinary differential equation (ODE) different to small caps!! (Fickett & Davis 1979). Given a fixed constant prestate, there is a minimum speed for the ZND profile, $D_{\mathrm{CJ}} > 0$, the Chapman–Jouguet velocity, and for every wave speed $D > D_{\mathrm{CJ}}$, there is a unique ZND profile moving with that wave speed. The parameter f defined according to :

$$\text{degree of overdrive } f = (D^2/D_{\mathrm{CJ}}^2) \tag{2.3}$$

measures the degree of overdrive of the detonation and satisfies $f \geqslant 1$. of a fixed ZND profile, a natural intrinsic length scale is the half-reaction length scale, the distance required for half the reactant to be depleted in the ZND wave. We always use the half-reaction length $L_{1/2}$ of the appropriate ZND wave as the unit length scale throughout the paper. We also normalize the sound speed in the unburnt medium to be $\sqrt{\gamma}$. With this normalization, the specification of $L_{1/2}$ as a length unit entirely determines the timescale and the normalization of K in the reaction rate w.

In figures 1 and 2 we illustrate the characteristics of ZND profiles in two examples. In figure 1 we plot the pressure and reactant profiles for a ZND wave with $E^+ = 20$, $q_0 = 2$, $f = 1.1$, $\gamma = 1.2$; we also graph the profile for $c^2(x) - v^2(x)$ where $c(x)$ is the sound speed and $v(x)$ is the normal velocity. In figure 2, we plot the same quantities for a ZND wave with $E^+ = 50$, $q_0 = 50$, $f = 1.2$,

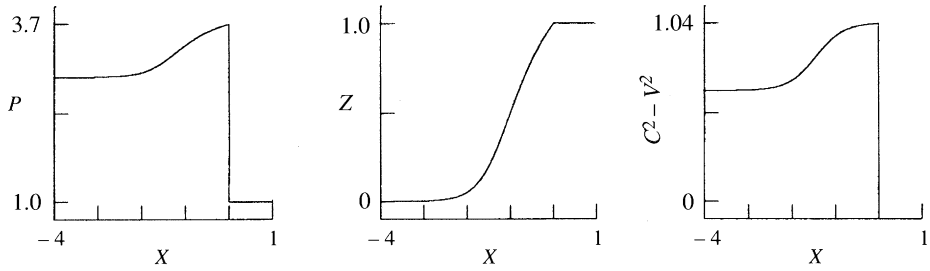

Figure 1. ZND profile with $E^+ = 20$, $q_0 = 2$, $f = 1.1$, $\gamma = 1.2$; pressure P, reactant mass fraction Z, and $c^2(x) - v^2(x)$, where $c^2(x)$ is the square of the sound speed and $v(x)$ is the normal velocity.

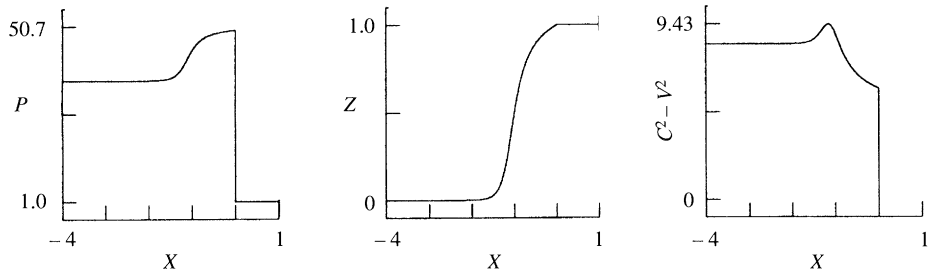

Figure 2. ZND profile with $E^+ = 50, q_0 = 50, f = 1.2, \gamma = 1.2$; pressure P, reactant mass fraction Z, and $c(x)^2 - v(x)^2$, where $c^2(x)$ is the square of the sound speed and $v(x)$ is the normal velocity.

$\gamma = 1.2$. Both ZND profiles exhibit the von Neumann spike in the pressure. Such non-monotone spikes increase the difficulty of numerical computations in reacting flows as compared with shocks in ordinary compressible flows. We also note that $c^2(x) - v^2(x)$ decreases in figure 1 but has an interior maximum in figure 2. This qualitative difference is very important since it signifies a quantitative difference in the instability characteristics of the ZND profile in figure 2 versus the one in figure 1. The profile in figure 1 with lower activation energy and heat release is stable at small transverse wavelengths while the profile in figure 2 is unstable at small transverse wavelengths (see § 4 below).

(*c*) *A qualitative–quantitative asymptotic model for detonation waves*

Several years ago, one of the authors introduced a qualitative model for dynamic combustion with two nonlinear equations which retains the essential interaction of nonlinear acoustics and chemistry essential for propagating detonations (Majda 1981). This simplified model has transparent analogues of the Chapman–Jouguet theory, ZND waves, some mechanisms of initiation-failure, etc., in an extremely simple context (see also Majda 1986; Majda & Roytburd 1988). It is interesting that this model actually arises from the reacting Euler equations in a distinguished asymptotic limit (Rosales & Majda 1983). In § 3, we illustrate the use of this model in testing numerical methods for computing detonations. Here we briefly sketch a derivation of the model and refer the reader to the original references for the complete details.

The model for high Mach number combustion has been derived from the reacting compressible Euler equations in (2.1) under the following hypotheses:

(i) The non-dimensional activation energy E^+ is high, of order $1/\epsilon$.

(ii) The non-dimensional heat release q_0 is small $q_0 = \bar{q}\epsilon^2$.

(iii) The perturbations of the reference state have amplitudes of order ϵ balanced with wave lengths of order ϵ.

The reaction front is described by the equation

$$\psi(x) - t = 0.$$

Using ideas of geometric optics, one can show that $\psi(x)$ should necessarily satisfy the eikonal equation:

$$|\nabla\psi|^2 = 1.$$

Near the reaction front appropriate inner asymptotic expansions for the state variables are introduced:

$$\begin{aligned}
\rho &= 1 + \epsilon\rho_0(\theta, x) + \dots \\
\boldsymbol{v} &= \boldsymbol{v}_0(\theta, x) + \epsilon\boldsymbol{v}(\theta, x) + \dots \\
T &= 1 + \epsilon T_0(\theta, x) + \dots \\
Z &= Z_0(\theta, x) + \epsilon Z_1(\theta, x) + \dots .
\end{aligned}$$

Here θ is a new scaled variable:

$$\theta = (\psi(x) - t)/\epsilon.$$

Enforcing appropriate solvability conditions, one shows that ρ_0, u_0, and T_0 solve a homogeneous system of equations; therefore these quantities should be proportional to some eigenvector:

$$\begin{pmatrix} \rho_0 \\ \boldsymbol{v}_0 \\ T_0 \end{pmatrix} = \begin{pmatrix} 1/(\gamma - 1) \\ \nabla\psi/(\gamma - 1) \\ 1 \end{pmatrix} U(x, \theta),$$

where $U(x, \theta)$ is a scalar function to be determined. We choose the eigenvector corresponding to propagating acoustic modes. From the next-order perturbation equations, a compatibility condition is found which yields a differential equation for U:

$$U_\tau + b(U^2/2)_\theta - q_0 Z_\theta + (\Delta\psi)U/2 = 0. \tag{2.4}$$

Here b is a constant and τ is a parameter on the bicharacteristic rays,

$$\frac{\mathrm{d}x}{\mathrm{d}\tau} = \nabla\psi(x)$$

with the initial condition

$$\tau = 0 \quad \text{at} \quad \psi(x) = 0.$$

The model system consists of (2.4) combined with the equation for Z:

$$U_\tau + b(U^2/2)_\theta - q_0 Z_\theta + (\Delta\psi)U/2 = 0, \quad Z_\theta = K\phi(U)Z. \tag{2.5}$$

In (2.5), ϕ accounts for the chemical kinetics; a typical choice for ϕ is the Arrhenius kinetic function:

$$\phi(U) = K \exp\{-E^+/(U - U_0)\}. \tag{2.6}$$

The effects of changing front geometry in multi-dimensions are included in the model via the term $(\Delta\psi)U/2$. This term can be expressed through principal curvatures K_j of the reaction front at time 0:

$$\Delta\psi = \sum_j K_j(1 + K_j\tau)^{-1}.$$

For the unidirectional motion of a planar front, the geometric term vanishes. The model ignores multi-wave interactions of gas dynamics but preserves the chemical nonlinear wave interaction along the dominant sound wave.

3. Stable and unstable ZND waves in one dimension

In this section we review recent developments in the interaction among theory, asymptotic, and numerical methods in understanding the instability of one-dimensional detonations. Problems in a single space variable provide important simplified testing grounds for the more sophisticated numerical and asymptotic methods needed for studying the more realistic situations involving detonation instability in two or three space variables. With this point of view, recent work has discovered a surprising number of purely numerical artefacts in solutions generated by existing numerical methods which are very successful for computing hydrodynamic shock waves without combustion. This work motivates the need for some of the new numerical strategies for computing unstable detonations which have been developed recently and are mentioned below. As reviewed here, the asymptotic theories play at least two roles in the development of improved numerical methods:

(i) Providing simplified systems for numerical studies such as those derived in (2.4), (2.5) through suitable asymptotic methods;

(ii) Yielding new theories for unstable detonation which can be compared with the results of direct numerical simulations in regimes where there are no 'exact solutions'. This provides stringent tests for the validity of numerical methods as well as these theories.

(*a*) *Linearized stability of ZND waves in one dimension*

The theory of linearized stability for ZND waves was pioneered by Erpenbeck (1962, 1964, 1969). Since the perturbed precursor shock front is also an unknown (even in a single space dimension), the linearized theory of stability for ZND waves involves a complex free surface problem for a variable coefficient system of linear hyperbolic equations. This system is solved by separation of variables in time, subject to suitable 'radiation conditions' in space. When at least one of the eigensolutions of this problem grow in time, the ZND profile is linearly unstable; otherwise, the ZND wave is stable. Here, we will not write down the equations for linearized stability of ZND profiles in a single space dimension; such equations are written down and developed in § 4 *a* in the context of several space variables and the situation involving a single space variable is obviously a very special case. Recently, Lee & Stewart (1990) have made an important contribution by developing a new shooting method for efficient numerical computation of the linearized stability theory for a given ZND profile. A careful discussion of the linearized problem in one dimension, including the 'radiation conditions' on eigenmodes, is needed (Lee & Stewart 1990; Bourlioux *et al.* 1991*a*,*b*). One

Table 1. *Roots for linear instability*
($q_0 = 50$, $E^+ = 50$, $\gamma = 1.2$. Roots are in units of $t_{1/2}^{-1}$, and an asterisk denotes a stable root.)

number of unstable modes	overdrive	root 1	root 2	root 3
0	1.8	$-0.0536 \pm i0.8362^*$	$-0.5846 \pm i4.0830^*$	$-1.7921 \pm i6.9913^*$
0	1.76	$-0.0230 \pm i0.8312^*$	$-0.4891 \pm i4.1346^*$	$-1.6277 \pm i7.0752^*$
0	1.74	$-0.0073 \pm i0.8280^*$	$-0.4401 \pm i4.1598^*$	$-1.5441 \pm i7.1250^*$
1	f_0^*=1.73	$0.0000 \pm i0.8263$	$-0.4153 \pm i4.1720^*$	$-1.5024 \pm i7.1506^*$
1	1.72	$0.0087 \pm i0.8243$	$-0.3903 \pm i4.1844^*$	$-1.4607 \pm i7.1767^*$
1	1.70	$0.0251 \pm i0.8199$	$-0.3398 \pm i4.2086^*$	$-1.3774 \pm i7.2292^*$
1	1.60	$0.1120 \pm i0.7902$	$-0.0760 \pm i4.3213^*$	$-0.9543 \pm i7.4853^*$
1	1.58	$0.1303 \pm i0.7821$	$-0.0207 \pm i4.3419^*$	$-0.8672 \pm i7.5341^*$
2	f_1^*=1.57	$0.1374 \pm i0.7788$	$0.0000 \pm i4.3496$	$-0.8233 \pm i7.5581^*$
2	1.56	$0.1491 \pm i0.7732$	$0.0350 \pm i4.3620$	$-0.7791 \pm i7.5819^*$
2	1.54	$0.1682 \pm i0.7636$	$0.0915 \pm i4.3810$	$-0.6901 \pm i7.6289^*$
2	1.50	$0.2078 \pm i0.7416$	$0.2065 \pm i4.4173$	$-0.5090 \pm i7.7198^*$
2	1.42	$0.2918 \pm i0.6837$	$0.4440 \pm i4.4794$	$-0.1359 \pm i7.8893^*$
2	1.40	$0.3140 \pm i0.6657$	$0.5055 \pm i4.4926$	$-0.0406 \pm i7.9290^*$
3	f_2^*=1.39	$0.3235 \pm i0.6575$	$0.5316 \pm i4.4978$	$0.0000 \pm i7.9456$
3	1.38	$0.3368 \pm i0.6460$	$0.5672 \pm i4.5047$	$0.0553 \pm i7.9676$
3	1.36	$0.3599 \pm i0.6242$	$0.6295 \pm i4.5159$	$0.1517 \pm i8.0049$
3	1.30	$0.4331 \pm i0.5433$	$0.8200 \pm i4.5422$	$0.4439 \pm i8.1095$
5	1.20	$0.5702 \pm i0.3003$	$1.5025 \pm i4.5267$	$1.4244 \pm i8.3517$

important feature of the numerical method is that the spatial structure of the eigenmode $e_+(x)$ corresponding to an unstable mode is also determined by the numerical procedure.

Table 1 lists the number of unstable modes for a given ZND profile with $E^+ = 50$, $q_0 = 50$, and $\gamma = 1.2$ as the overdrive, f (defined in 2.3), is varied. We remark that the number of unstable modes is calculated according to a complex field so that there are twice as many real-valued unstable modes in the unstable cases. From table 1 we see that the ZND profile becomes increasingly more unstable as the overdrive is decreased and that

(A) the ZND profile is linearly stable for $f > f_0^* = 1.73$ and unstable for $f < f_0^*$.

The three roots with the largest growth rates for each overdrive are also recorded in table 1.

(b) Numerical computation of stable ZND waves

The simplest task for a numerical scheme for computing detonations is to capture a stable ZND profile including the non-monotone von Neumann spike in the pressure profile. The performance of several contemporary 'shock-capturing' schemes on such problems has been documented recently (Colella *et al.* 1986; Ben-Artzi 1989; LeVeque & Yee 1990; Bourlioux 1991).

(i) *Artefact numerical weak detonations*

The most surprising behaviour of numerical methods (Colella *et al.* 1986) is that numerical artefact precursor weak detonations can emerge on sufficiently coarse meshes in a time-dependent calculation rather than the stable overdriven or Chapman–Jouguet detonation. That the weak detonation waves are purely numerical artefacts follows from the fact that their wave speed depends on the mesh spacing. Also these meshes are coarse for the reactive Euler equations but the same mesh spacings yield high-quality resolution for shock capturing for the compressible Euler equations without chemistry. Thus, the interaction of the stiff chemical source terms with gas dynamics can produce surprising numerical artefacts which pollute the computation.

A theory and explanation for these artefact waves is presented in Colella *et al.* (1986) within the context of the simplified asymptotic model in (2.4), (2.5). Recently, LeVeque & Yee (1990) have made an important contribution by observing the same kind of numerical artefact waves moving at the wrong speed for an even simpler system involving a scalar linear advection equation with a stiff nonlinear source term. Clearly, one important design consideration for numerical schemes for calculating detonations is that such numerical artefact precursor weak detonations be eliminated for the grid spacings that are limited by expense in a more complex calculations.

(ii) *Numerical schemes tested on the asymptotic model*

The ZND profiles in the simplified asymptotic model in (2.4), (2.5) provide a simple but instructive class of code validation problems where many different numerical methods can be compared readily. Table 2 lists the performance of eight contemporary shock-capturing schemes combined with operator splitting applied to a test problem for a Chapman–Jouguet profile with prestate zero for the simplified equations in (2.4), (2.5), (2.6) with $b = 1$, $u_0 = 0.6$, $E^+ = 10$, $q_0 = 0.5$ (Bourlioux 1991). These calculations were performed on a Ridge computer and the timings for each method are for piecewise constant initial values run for a fixed time interval for the solution. The random choice method (RCM) (Chorin 1976), flux corrected transport method (FCT) (Boris & Book 1973), and the piecewise parabolic method (PPM) (Colella & Woodward 1984) gave the best overall results on this simple test problem. In fact, RCM gave a perfect shock speed and only slightly clipped the von Neumann spike. The scheme ENO4 (Harten *et al.* 1987) gave similar results but was significantly more expensive to use.

Several more stringent but elementary one-dimensional test problems involving initiation and failure within the context of the model as well as for the reactive Euler equations (Majda & Roytburd 1990; Bourlioux 1991) have also been used to check numerical performance. The three schemes RCM, FCT, and PPM with operator splitting gave the best performance on all of these test problems.

PHILOSOPHICAL TRANSACTIONS OF THE ROYAL SOCIETY A MATHEMATICAL, PHYSICAL & ENGINEERING SCIENCES

Table 2. *Effect of mesh refinement*
($E^+=10$; $Q_0=0.5$.)

method	pts/$L_{1/2}$	$L_1(u)$	clipping	shock speed	shock spread	timing
RCM	1	0.55	3.62%	0.960	0.00 pts	10.1
	2	0.24	2.09%	0.980	0.00 pts	20.2
	4	0.12	1.08%	0.988	0.00 pts	40.4
FCT	1	1.28	9.58%	0.994	1.34 pts	15.1
	2	0.66	6.51%	0.997	1.37 pts	30.5
	4	0.33	4.44%	0.999	1.38 pts	1:01.6
PPM	1	1.31	8.54%	0.997	1.54 pts	12.5
	2	0.75	5.58%	0.996	1.63 pts	25.1
	4	0.44	3.53%	0.998	1.73 pts	50.4
Superbee	1	1.31	8.67%	0.994	1.63 pts	12.4
	2	0.78	5.64%	0.996	1.76 pts	25.1
	4	0.44	3.55%	1.000	1.84 pts	50.6
ENO4	1	1.18	10.88%	0.995	1.62 pts	2:14.0
	2	0.69	6.96%	0.998	1.73 pts	4:20.3
	4	0.41	4.32%	1.000	1.82 pts	8:38.4
ENO2	1	1.78	10.98%	0.994	2.39 pts	37.3
	2	1.05	7.13%	0.999	2.53 pts	1:14.4
	4	0.63	4.60%	0.999	2.69 pts	2:28.1
GOD	1	1.98	10.63%	0.994	2.60 pts	10.2
	2	1.16	7.29%	0.996	2.79 pts	20.5
	4	0.69	4.87%	1.000	3.03 pts	40.9
TVD	1	2.81	12.72%	0.996	2.96 pts	14.4
	2	1.58	8.28%	1.000	3.11 pts	28.6
	4	0.86	5.11%	1.000	3.22 pts	56.9

(*c*) *Numerical computation of unstable ZND waves*

Since most detonation waves which occur in applications are unstable and the corresponding higher pressures have physical significance, a real computational challenge is to design high-resolution numerical methods for computing the interactions between the chemical reactions and hydrodynamics for unstable detonations. Fickett & Wood (1966) introduced two important classical test problems for unstable detonations in a single space variable by considering the instability

of ZND waves with $q_0 = 50, E^+ = 50, \gamma = 1.2$ and the two overdrives $f = 1.6$, 1.8. From table 1, the reader can verify that the ZND wave with $f = 1.6$ is unstable with a single mode of growth while at $f = 1.8$, the ZND wave is stable but there is one mode with a slow rate of decay. After the first publication of this test problem, several authors (Mader 1979; Abouseif & Toong 1982; Moen *et al.* 1984; Bukiet 1987) have used this test problem in theoretical and numerical studies; their work involves using extremely fine mesh spacings in one space dimension; comparable mesh spacings are not available for simulations in two space dimensions on even the largest current supercomputers.

Recently, Bourlioux *et al.* (1991*a*) investigated the performance of numerical methods on the unstable and stable one-dimensional detonations of Fickett and Wood with the following design consideration:

(B) Find a 'state of the art' numerical method which generalizes to several space dimensions and accurately computes the transition to instability for overdrives with $1.6 \leqslant f \leqslant 1.8$ with a coarse resolution using only $O(10^3)$ mesh points.

If such a method can be found, then this method provides a new high-resolution numerical procedure for unstable detonations in two space dimensions where $O(10^6)$ mesh points are available on contemporary supercomputers.

(i) *Numerical artefacts for the classical test problem*

With the design considerations in (B), the numerical performance of the RCM, FCT, and PPM methods was studied (Bourlioux *et al.* 1991*a*) on the classical test problem of Fickett & Wood with the relatively coarse resolutions involving 2 pts/$L_{1/2}$, 5 pts/$L_{1/2}$, 10 pts/$L_{1/2}$ three numerical methods was based on their superior performance in the simpler test problems already described in § 3 *b* (ii). In figure 3, we give the shock front pressure history for the 'exact solution' computed from a very fine mesh calculation for the unstable overdrive, $f = 1.6$; clearly, a regular periodic pulsating mode of instability emerges after a brief time.

For numerical simulations with initial data given by the unperturbed ZND wave, both the FCT method and the RCM method exhibited dramatic numerical artefacts as the mesh was refined and these persisted and in some instances were even exaggerated as the mesh spacing was reduced. Figure 4 gives the shock front pressure history for the FCT method with the unstable overdrive, $f = 1.6$. On the coarsest mesh with 2 pts/$L_{1/2}$, the ZND wave is computed as a stable detonation as a purely numerical artefact; the PPM method behaves similarly on this very coarse mesh. On the middle mesh with 5 pts/$L_{1/2}$, periodic pulsations emerge with maximum pressures about 10% below the expected value from figure 3. On the finest mesh with 10 pts/$L_{1/2}$, the numerical viscosity is reduced and new numerical artefacts emerge as a consequence of the anti-diffusive numerical step in FCT (Oran & Boris 1987). The shock front pressure history develops non-physical localized spikes with amplitudes exceeding 140 and even non-physical negative density states in the corresponding spatial profile beyond the time $t = 25$. For the calculations reported in figure 4, a CFL number of 0.25 was used; when the recommended CFL number of 0.50 was used, the FCT method 'blew up' and gave overflow from an exaggerated version of the same numerical effect. Other serious numerical artefacts occurred in FCT for the stable case with overdrive $f = 1.8$;

PHILOSOPHICAL TRANSACTIONS OF THE ROYAL SOCIETY A MATHEMATICAL, PHYSICAL & ENGINEERING SCIENCES

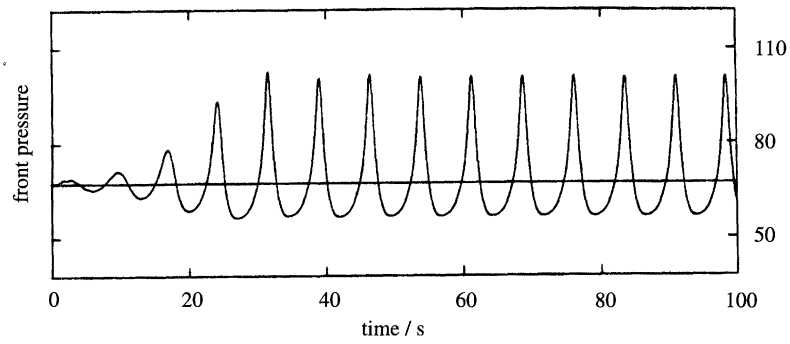

Figure 3. Shock pressure history for the one-dimensional unstable detonation $E^+ = 50$, $q_0 = 50$, $f = 1.6$, $\gamma = 1.2$.

the FCT method treated this stable detonation as if it was unstable for these mesh sizes.

The PPM method definitely gave the best results of the three methods and, in contrast to RCM and FCT, treated both the stable and unstable cases correctly on the two finer meshes. For PPM the effects of numerical viscosity were clearly evident on all but the finest mesh with 10 pts/$L_{1/2}$ in the unstable case; the pressure maxima were clipped by 10% with 5 pts/$L_{1/2}$. Unfortunately, a resolution of 10 pts/$L_{1/2}$ requires 5×10^3 mesh points for even comparatively short time runs; thus running PPM with this resolution in general investigations of detonation instability in two space dimensions is not possible with even the largest contemporary supercomputers.

(ii) *A new numerical method for unstable detonations*

Based on the computational experiments documented above, a new numerical method for computing unstable detonations in a single space dimension was developed and thoroughly tested. The basic structure of a fractional step scheme is retained. In the first fractional step, the hydrodynamic part of the problem is solved and the mass fraction of the reactant is advected as a passive scalar; in the second fractional step, the species equation is advanced explicitly by integrating the ODE for the mass fraction given the temperature field from the previous fractional step. The hydrodynamic solver incorporates three ingredients in the basic code:

(C) (i) a higher-order Godunov scheme such as PPM as the basic conservative difference scheme;
(ii) conservative shock tracking of the leading detonation front;
(iii) adaptive mesh refinement in the region of stiff chemical energy release in the vicinity of the precursor shock front.

The choice of higher-order Godunov schemes such as PPM as the basic conservative difference scheme is motivated by the superior behaviour of this method on the test problems. The use of conservative front tracking was motivated by the fact that PPM clips the basic leading front on coarse meshes and the physical instabilities are generated by interactions with this leading shock front. The use of adaptive mesh refinement in (2.4) gives an economical representation of the solution since much coarser meshes can be used in the regions without significant

PHILOSOPHICAL TRANSACTIONS OF THE ROYAL SOCIETY A MATHEMATICAL, PHYSICAL & ENGINEERING SCIENCES

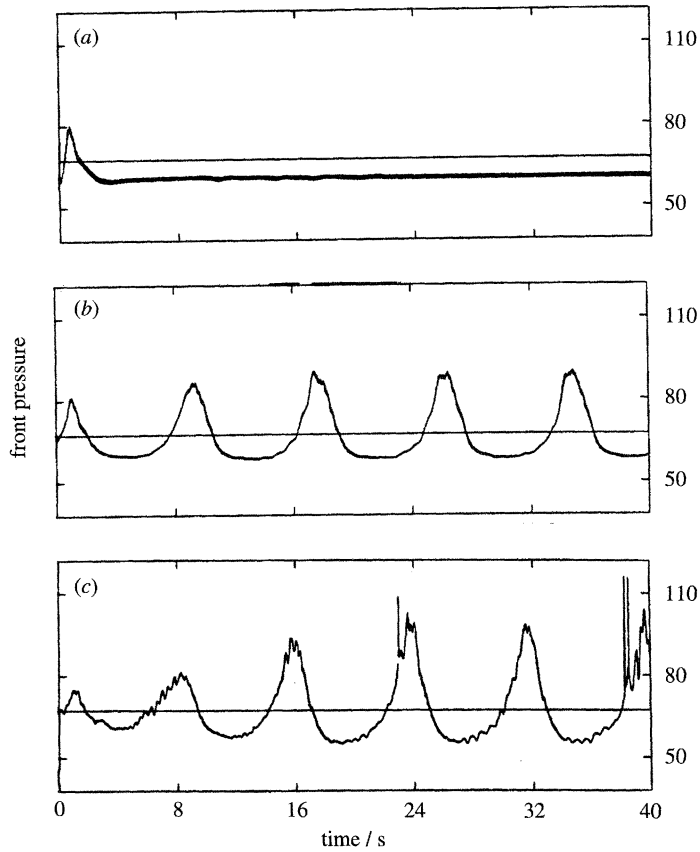

Figure 4. Mesh refinement study with FCT of the shock pressure history for the one-dimensional unstable detonation $E^+ = 50$, $q_0 = 50$, $f = 1.6$, $\gamma = 1.2$.

combustion. The numerical algorithm meets the design requirements in (B) and generalizes readily to two space dimensions. We discuss this important generalization in § 5 *a* of this review. In § 3 *e*, we indicate the fashion in which asymptotic theories and this new robust numerical method can be used to elucidate the structure of unstable one-dimensional detonations.

(*d*) *Asymptotic theory for detonation instability in one dimension*

The trends in table 1 illustrate a general fact that detonations become more unstable as the overdrive decreases. This suggests that decreasing the overdrive, f, plays the role of a bifurcation parameter, much like increasing the Reynolds number in fluid dynamics, so that asymptotic ideas and techniques from hydrodynamic stability theory can be adapted to develop asymptotic theories for the dynamic development of instability in detonations. The simplest example of such theories involves the dynamic development of instabilities in one-dimensional detonations for overdrives with $f < f_0^*$ and $f_0^* - f \ll 1$ where ZND waves are stable for overdrives with $f > f_0^*$ and unstable for $f < f_0^*$ provided the heat release and activation energy are fixed. The example in (A) satisfies these requirements with $f_0^* = 1.73$. A detailed asymptotic theory for this situation has been developed recently (Bourlioux *et al.* 1991*b*) and is summarized next.

We use the vector notation $u = {}^t(\rho, v, p, Z)$. The precursor shock in the perturbed ZND profile in the laboratory reference frame is given by

$$x = \psi(t). \tag{3.1}$$

We denote by $\boldsymbol{e}(x, f)$, the eigenmode for the linearized ZND profile with the largest growth rate at overdrive f. We consider overdrives f with $f < f_0^*$ and

$$f_0^* - f = \epsilon^2 \tag{3.2}$$

with ϵ a small parameter and $\epsilon \ll 1$; at these overdrives the ZND profile is linearly unstable. The asymptotic procedure systematically builds asymptotic solutions of the reacting compressible Euler equations in (2.1) given by a constant state ahead of the shock and with the form,

$$\left.\begin{aligned} \psi &= Dt + \tfrac{1}{2}[\epsilon A(\epsilon^2 t)\mathrm{e}^{\mathrm{i}\omega t} + \epsilon^2 \psi^{(2)}] + \tfrac{1}{2}[\text{c.c.}], \\ u &= u^0 + \tfrac{1}{2}[\epsilon A(\epsilon^2 t)\mathrm{e}^{\mathrm{i}\omega t}\boldsymbol{e}(x', f) + \epsilon^2 u^{(2)}] + \tfrac{1}{2}[\text{c.c.}], \end{aligned}\right\} \tag{3.3}$$

behind the precursor shock, where c.c. denotes complex conjugate and the coordinates x' are shock attached coordinates. Here u^0 denotes the unperturbed ZND profile with speed D at overdrive f. The frequency ω is the imaginary part of the corresponding eigenvalue in the right half-plane for the given overdrive f. The systematic asymptotic procedure automatically predicts that the amplitude function $A(T)$ solves a Landau–Stuart equation,

$$\mathrm{d}A/\mathrm{d}T = \chi A + \beta A^2 \bar{A}, \tag{3.4}$$

where β and χ are constants systematically determined by the asymptotic procedure with

$$\chi > 0, \quad \operatorname{Re}\beta < 0. \tag{3.5}$$

Next we describe the predictions of dynamic detonation instability by using the elementary behaviour of solutions of (3.7). With polar coordinates

$$A(T) = R(T)\mathrm{e}^{\mathrm{i}\theta(T)} \tag{3.6}$$

the equation in (3.7) becomes

$$\mathrm{d}R(t)/\mathrm{d}t = \chi R(t) + (\operatorname{Re}\beta)R^3(t), \quad \mathrm{d}\theta(t)/\mathrm{d}t = (\operatorname{Im}\beta)R^2(t). \tag{3.7}$$

With (3.8), the first equation in (3.10) has two steady states for $R(t) \geqslant 0$, namely

$$R(t) \equiv 0 \quad \text{and} \quad R_+ \equiv (\chi/|\operatorname{Re}\beta|)^{1/2}. \tag{3.8}$$

Furthermore, the reader can easily check that every solution $R(t) \neq 0$ of the first equation in (3.10) tends to the steady state R_+ as time increases; in fact the first equation in (3.10) has an explicit solution by quadrature (Drazin & Reid 1981). The second equation for the phase in (3.10) is readily integrated once $R(t)$ is known.

What do these facts yield for the predictions by the asymptotic theory of the instability process? We see from (3.6) that the unstable critical point with $R(t) \equiv 0$ corresponds to the basic unperturbed ZND wave. On the other hand, the stable critical point R_+ gives the non-zero solution,

$$A(T) = (\chi/|\operatorname{Re}\beta|)^{1/2}\,\mathrm{e}^{\mathrm{i}(\chi/|\operatorname{Re}\beta|)T}, \tag{3.9}$$

and every solution with $R(T)|_{t=0} \neq 0$ tends to the solution in (3.12). By inserting (3.12) into the asymptotics in (3.6), we generate an asymptotic prediction of an oscillating periodic shock front pressure history with the same qualitative form as given in figure 3. Furthermore, the asymptotic theory predicts a perturbed spatial structure determined by the linearized eigenmode, $\boldsymbol{e}(x', f)$.

The reader familiar with nonlinear hydrodynamic stability theory (Drazin & Reid 1981, ch. 7) above instability is a Hopf bifurcation: a pair of complex conjugate eigenvalues cross the real axis into the unstable half-plane as the overdrive decreases through f_0^*. Nevertheless, this is a non-classical Hopf bifurcation because resonant acoustic scattering states with exponential growth in space cross the imaginary axis and become unstable nonlinear eigenmodes. While the general outline of the asymptotic procedure follows ideas of hydrodynamic stability theory, the actual details in deriving (3.6) and (3.7) are very different because of the unusual and complicated structure of the linearized operator and the necessity of finding the appropriate unique adjoint operator. In fact, earlier attempts at nonlinear stability theory for unstable detonations (Erpenbeck 1966, 1970) suffer from the defect that this unique adjoint problem was never used in a systematic fashion with the unsatisfactory consequence that the differential equation for the amplitude $A(T)$ was never specified uniquely, that it had an almost arbitrary form, and that secularities in the asymptotics were not suppressed. Erpenbeck (1966) himself noted this ambiguity in his asymptotic procedures.

(*e*) *Interaction of asymptotic theory and numerics in predicting one-dimensional detonation instability*

The asymptotic theory just summarized in § 3 *d* provides a detailed prediction for both the growth and spatial structure of the instability for overdrives in the vicinity of $f_0^* = 1.73$ for the family of test problems discussed in (B). The asymptotic theory provides a significant prediction which can be validated by numerical simulations; furthermore, a glance at the extremely small growth and decay rates of significant eigenmodes in table 1 in the vicinity of the critical overdrive $f_0^* = 1.73$ indicates that these are challenging one-dimensional problems to check the capability of numerical methods to detect instability. The numerical method described in § 3 *c* (ii) and several facets of the asymptotic theory described in § 3 *d* were checked with excellent agreement (Bourlioux *et al.* 1991*a*). Below we briefly describe one such comparison.

In figure 5, we display results for the *unstable case* $f = 1.70 < f_0^*$. The plot in figure 5*a* gives the time evolution of *the pressure at the shock*. The plot shows how the original small perturbation, which is essentially due to the truncation error of the numerical scheme, gradually increases in magnitude to approach some asymptotic saturation level. Simultaneously the pressure experiences oscillations about the ZND value which is shown by a horizontal line. The period of these oscillations is very close to the one determined by the linearized unstable frequency $\mathrm{Im}(\alpha(f)) = 0.82$.

In figure 5*b* we display the perturbed pressure and specific volume profiles from the numerical simulation at the time $t = 65.6$. The left half of figure 5*b* gives the spatial profiles for a distance of 400 half-reaction lengths from the leading shock while the right-hand side reveals a more detailed picture of the first 20 units behind the shock. We determined the perturbation profiles by subtracting the exact values of the steady ZND profile from the *computed solution*

PHILOSOPHICAL TRANSACTIONS OF THE ROYAL SOCIETY A MATHEMATICAL, PHYSICAL & ENGINEERING SCIENCES

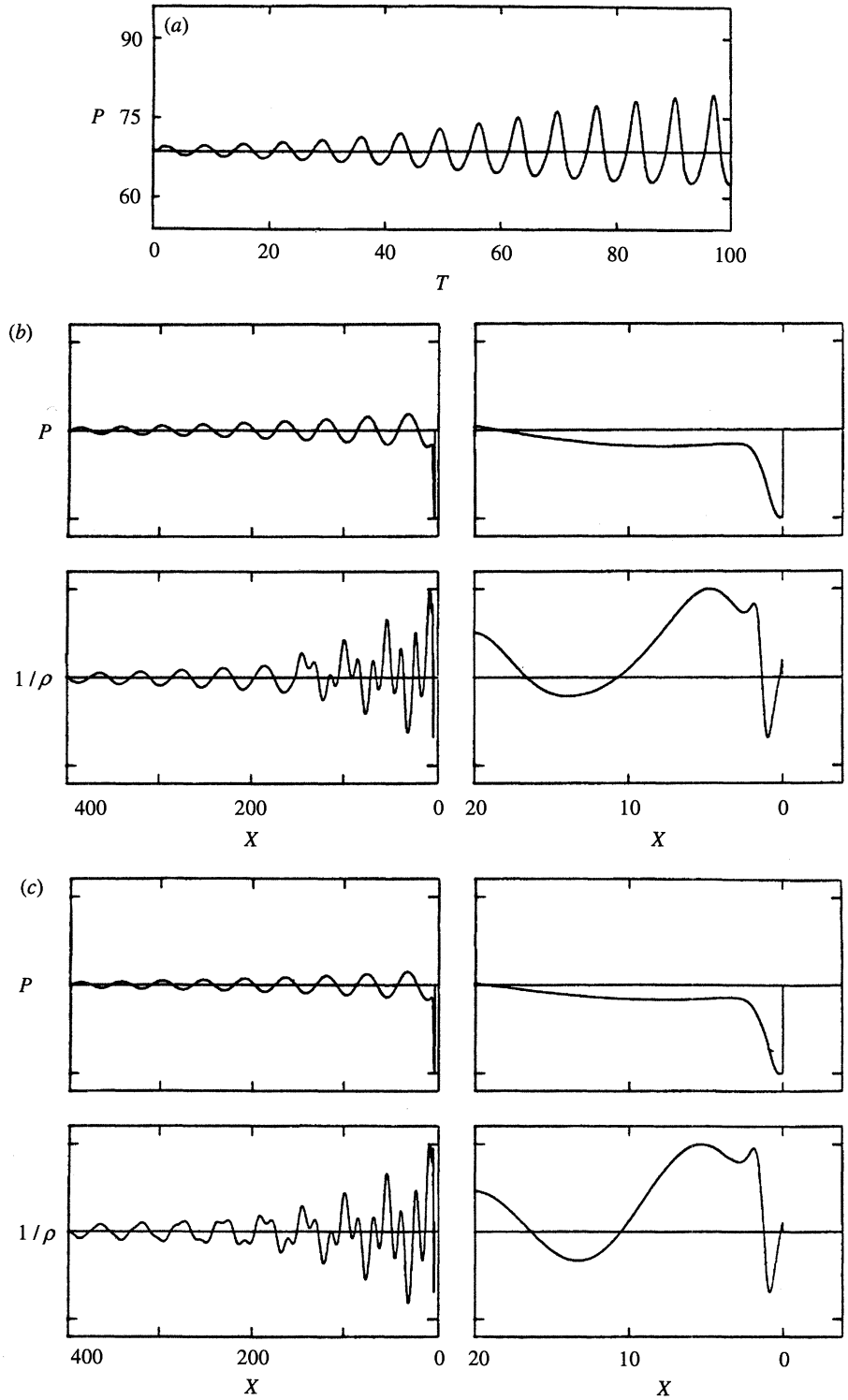

Figure 5. One-dimensional unstable detonation $E^+ = 50$, $q_0 = 50$, $f = 1.7$, $\gamma = 1.2$: (a) shock pressure history; (b) direct simulation; (c) linearized eigenfunction.

PHILOSOPHICAL TRANSACTIONS OF THE ROYAL SOCIETY A MATHEMATICAL, PHYSICAL & ENGINEERING SCIENCES

and then scaled amplitudes by the same scale that is used in figure 5*c* where the corresponding components of the linearized eigenfunction are presented. The agreement between the two sets of profiles in figure 5*b*,*c* is really remarkable. Even the complicated oscillatory structure of the specific volume on large length scales exhibits rather close agreement between theory and computation. We have omitted spatial profiles for other state variables which also demonstrate a very good agreement. These results confirm the validity of both the theory and the numerical computations described here.

4. Theories for detonation instability in multi-dimensions

In this section we review some of the classical and current developing theories for detonation instability in several space dimensions. We include a discussion of linear and nonlinear theories for instability in both low-frequency and short-wavelength regimes and the connections among these theories that have been developed recently. In § 5 we will illustrate the fashion in which these theories interact with numerical computations to give new insights into the instability of detonations in two space dimensions.

(*a*) *Linearized instability of ZND waves in multi-dimensions*

The theory of linearized stability for ZND waves in multi-dimensions was developed by Erpenbeck (1962, 1964, 1969) and this last reference remains an important summary and discussion of this work. We will make several comments in § 4 *b* on some of the recent developments that have clarified some of the issues then, particularly as regards short wavelength transverse instabilities and geometric acoustics.

We begin with a sketch of the procedure for obtaining the equations for the linear stability analysis of ZND profiles in two space dimensions. Since there is rotational invariance in the directions transverse to the ZND wave, this two-dimensional situation also automatically covers the general three-dimensional case as regards linearized stability analysis. We change the notation for the variables in equation (2.1) slightly here for convenience in exposition but this should not confuse the reader. In the laboratory coordinate system (x^{l}, y, t), the shock front location is described by a curve $x_{\mathrm{s}} = D_{\mathrm{s}}t + \psi(y,t)$, where D_{s}, is the ZND shock speed. We transform the basic equations in (2.1) to the shock attached coordinates (x, y, t) where

$$x = x^{\mathrm{l}} - D_{\mathrm{s}}t - \psi(y,t). \tag{4.1}$$

In the new coordinate system, the shock is described by the straight line $x = 0$. If we define u_1 to be the particle velocity x-component in the steady frame

$$u_1 = u_1^{\mathrm{l}} - D_{\mathrm{s}} \tag{4.2}$$

the governing equations are now written

$$z_t + Az_x + Bz_y - \psi_t b - \psi_y Bb = c, \tag{4.3}$$

where

$$z = \begin{pmatrix} v \\ u_1 \\ u_2 \\ p \\ \lambda \end{pmatrix}, \quad b = z_x, \quad c = \begin{pmatrix} 0 \\ 0 \\ 0 \\ (\gamma - 1)Q_0 r/v \\ r \end{pmatrix}, \tag{4.4}$$

$$A = \begin{pmatrix} u_1 & -v & 0 & 0 & 0 \\ 0 & u_1 & 0 & v & 0 \\ 0 & 0 & u_1 & 0 & 0 \\ 0 & \gamma p & 0 & u_1 & 0 \\ 0 & 0 & 0 & 0 & u_1 \end{pmatrix}, \quad B = \begin{pmatrix} u_2 & 0 & -v & 0 & 0 \\ 0 & u_2 & 0 & 0 & 0 \\ 0 & 0 & u_2 & v & 0 \\ 0 & 0 & \gamma p & u_2 & 0 \\ 0 & 0 & 0 & 0 & u_2 \end{pmatrix}. \tag{4.5}$$

Here v is the specific volume, u_1 and u_2 are the two velocity components, p is the pressure and $\lambda = 1 - z$ is the mass fraction of burnt gas. We linearize the above equations, assuming a normal mode expansion and Fourier transform in the transverse direction

$$z = z^*(x) + z'(x)\exp(\alpha t)\exp(\mathrm{i}ky), \quad \psi = \psi' \exp(\alpha t)\exp(\mathrm{i}ky), \tag{4.6}$$

where the prime superscript refers to a small perturbation while a star denotes the basic ZND values. The linearized perturbation equations are

$$\alpha z' + A^* z'_x + \mathrm{i}kB^* z' + C^* z' - \alpha b^* \psi' - \mathrm{i}kB^* b^* \psi' = 0, \tag{4.7}$$

where

$$C = \begin{pmatrix} -u_{1x} & v_x & 0 & 0 & 0 \\ p_x & u_{1x} & 0 & 0 & 0 \\ 0 & 0 & 0 & 0 & 0 \\ -\dfrac{(\gamma-1)}{v} Q_0 \left[r_v - \dfrac{r}{v} \right] & p_x & 0 & \gamma u_{1x} - \dfrac{(\gamma-1)}{v} Q_0 r_p & -\dfrac{(\gamma-1)}{v} Q_0 r_\lambda \\ -r_v & \lambda_x & 0 & -r_p & -r_\lambda \end{pmatrix}. \tag{4.8}$$

The linearized Rankine–Hugoniot shock jump conditions for v, u_1, p, λ are as follows: the continuity of the component of the velocity tangential to the shock gives

$$u'_2 = -u_1^* \psi_y. \tag{4.9}$$

The shock conditions can be written as

$$\left.\begin{aligned} v'_2 &= -\frac{4}{(\gamma+1)M_s^3\sqrt{\gamma}}\alpha\psi', \quad u'_{1s} = \frac{2M_s^2+2}{(\gamma+1)M_s^2}\alpha\psi', \\ u'_{2s} &= -2\sqrt{\gamma}\,\frac{M_s^2-1}{(\gamma+1)M_s}\mathrm{i}k\psi', \quad p'_s = \frac{4\sqrt{\gamma}\,M_s}{(\gamma+1)}\alpha\psi', \quad \lambda'_s = 0, \end{aligned}\right\} \tag{4.10}$$

with M_s the Mach number at the unperturbed precursor shock. The equations in (4.7) and (4.10) need to be supplemented by a 'radiation condition' which has the physical content that perturbations are not allowed to come in from infinity behind the shock and affect the stability; this is a causality condition which guarantees that the number of boundary conditions in (4.10) exactly matches the number of solutions of (4.7) satisfying the causality condition.

The basic ZND profile is unstable in multi-dimensions provided there is a wave number k, a complex number $\alpha(k)$ with growth rate $\mathrm{Re}(\alpha(k)) > 0$, and a spatial eigenmode $\boldsymbol{e}(x,k)$ so that with $\psi' = 1$ and $z' = \boldsymbol{e}(x,k)$, these functions satisfy the equations in (4.7) and (4.10). The special case when the transverse wave number vanishes, so $k = 0$, defines the equations for the linearized instability of a ZND wave in a single space dimension. Clearly ZND waves can be unstable in multi-dimensions at transverse wave numbers without necessarily being unstable in the normal direction corresponding to a one-dimensional stability analysis. An

PHILOSOPHICAL TRANSACTIONS OF THE ROYAL SOCIETY A MATHEMATICAL, PHYSICAL & ENGINEERING SCIENCES

Figure 6

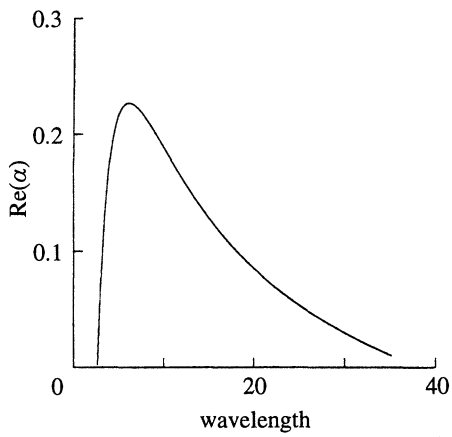

Figure 7

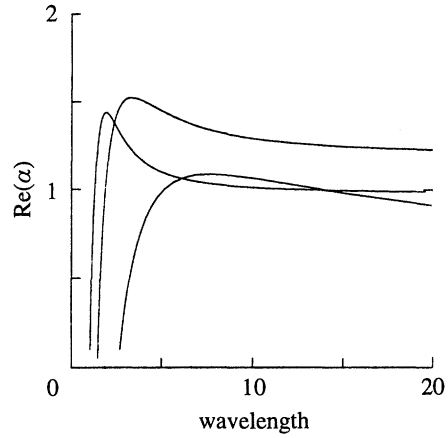

Figure 6. Simple linear stability diagram (one family of unstable modes corresponding to one curve for the growth rate $\mathrm{Re}(\alpha)$ as a function of the transverse wavelength W). $E^+ = 10$; $q_0 = 50$; $f = 1.2$.

Figure 7. Complex linear stability diagram (shown are three distinct branches of unstable modes corresponding to three curves for the growth rate $\mathrm{Re}(\alpha)$ as a function of the transverse wavelength W). There are many more unstable branches extending to $W = 0$ because this detonation is short-wavelength unstable. $E^+ = 50$; $q_0 = 50$; $f = 1.2$.

example will be given below. One of the authors (Bourlioux 1991) has adapted the numerical shooting procedure of Lee & Stewart (1990) to compute both the transverse wave numbers, k, of instability as well as the spatial structure of the eigenmode, $\boldsymbol{e}(x, k)$, in the linearized stability analysis. Such additional structure is useful in providing initial data to systematically perturb ZND profiles in numerical simulations (see § 5).

In figures 6 and 7 we present the stability diagrams for two detonations with the same heat release and overdrive but different activation energies. We use the heat release, $q_0 = 50$, overdrive, $f = 1.2$, and $\gamma = 1.2$. In figure 6, the activation energy is $E^+ = 10$ while $E^+ = 50$ for figure 7. The graphs in the figures plot $\mathrm{Re}(\alpha)$ as a function of transverse wavelength. We note that $W = 2\pi/k$ where k is the transverse wave number so that small wave numbers correspond to $W \to \infty$ in figures 6 and 7. The graph in figure 6 indicates that for the lower activation energy, the ZND profile has simple instability characteristics; there is a single curve of unstable modes with a simple maximum at $W \approx 6$ and the unstable modes are all concentrated at long transverse wavelengths. Nevertheless, this ZND wave is stable with respect to one-dimensional normal perturbations since there is clearly no growth at $k = 0$ ($W \to \infty$ in figure 6). The graph in figure 7 reveals a much more complex stability diagram for the ZND wave with $E^+ = 50$. Three unstable branches are plotted in figure 7 and it is known (Erpenbeck 1969) that the modes of instability extend to arbitrarily small transverse wavelengths. Figure 7 indicates that the ZND wave in figure 7 is also unstable in a single space variable since growth persists as $W \to \infty$. This is confirmed by the listing for overdrive $f = 1.2$ in table 1.

Obviously, the general theory of linearized stability for ZND waves is very complicated and this led Erpenbeck (1966, 1969) to develop a simpler criterion for detonation instability at arbitrarily small transverse wavelengths.

PHILOSOPHICAL TRANSACTIONS OF THE ROYAL SOCIETY A MATHEMATICAL, PHYSICAL & ENGINEERING SCIENCES

(*b*) *Geometric acoustics and detonation instability*

The role of trapping of short-wavelength acoustic signals in detonation instability was pioneered by Strehlow and his co-workers (Strehlow & Fernandes 1965; Barthel & Strehlow 1966; Barthel 1974; Strehlow 1978). Recently, Majda (1987) has developed a more complete geometric theory of detonation instability through a systematic use of the theory of high-frequency geometric optics. This theory was motivated strongly by the earlier work and generalizes it by including all explicit time-dependent amplifying mechanisms as well as nonlinearity for small-amplitude high-frequency wave patterns with ray trapping. This theory also provides explicit physical mechanisms which lead to translating amplifying self-similar transverse wave patterns with small-amplitude waves which resemble the regular patterns for Mach stems and yields explicit criteria for cell spacing generalizing those proposed earlier. It also establishes a link between the above physical theories of detonation instability through geometric acoustics and Erpenbeck's complex formal theory of short-wavelength linearized instability and answers a question posed by Erpenbeck (1969). Namely, for a given ZND wave profile, self-similar amplifying short-wavelength patterns of geometric acoustics occur if and only if the ZND profile satisfies Erpenbeck's explicit algebraic conditions for short-wavelength instability. Some additional algebraic details establishing this link are presented by Bourlioux (1991).

Two conditions are necessary in order for the theory of geometric acoustics to predict detonation instability:

(D) (i) trapped acoustic rays occur;
(ii) amplification of acoustic amplitudes should occur in one complete reflection cycle along the trapped rays.

Next, we discuss the conditions in (D) as background for the numerical experiments.

The quantity $c^2(x)-v^2(x)$ determines the ray trapping where $c(x)$ is the sound speed and $v(x)$ is the normal velocity in the unperturbed ZND profile. Erpenbeck classifies ZND profiles according to the behaviour of this quantity into three groups:

(E) (i) For type D (decreasing) profiles, $c^2(x)-v^2(x)$ decreases monotonically from the shock and no rays are trapped.
(ii) For type M (maximum) profiles, $c^2(x)-v^2(x)$ has a unique maximum at $\hat{x}$ and there is a continuous band of trapped rays.
(iii) For type I (increasing) profiles, $c^2(x)-v^2(x)$ increases with the maximum at infinity and there is a continuous band of trapped rays.

Thus, from (D), ZND profiles need to be of type M or I in order to be unstable at high wave numbers and have trapped rays. Of course, not every ZND profile of type M or I satisfies condition (ii) of (D) and yields acoustic wave amplification in one reflection cycle. In any given ZND profile, the explicit formulas from Majda (1987) guaranteeing the amplification of wave patterns from geometric acoustics can be determined by numerical quadrature: for a given heat release q_0 and overdrive ratio f, the condition for amplification of the acoustic perturbation is that the activation energy E^+ be larger than some transition value $E^+_{\mathrm{tr}}(q_0, f)$. Also the transverse distance y travelled by a given amplifying wave pattern is readily calculated numerically. The ZND profiles from figures 6 and 7 are type M

profiles. For the activation energy $E^+ = 50$, this is clear from figure 2. In figure 6, the activation energy $E^+ = 10$ is smaller than the transition value $E^+_{tr} = 11.1$ at $q_0 = 50, f = 1.2$, and the trapped rays cannot amplify. In figure 7, $E^+ = 50$ and the detonation is unstable at short wavelengths: there is a band of translating amplifying self-similar transverse acoustic wave patterns. This ZND profile has the typical structure assumed by Strehlow. On the other hand, the ZND wave with the structure from figure 1 has a type D profile and is stable at small transverse wavelengths.

(c) *Theoretical predictions for cell spacing via detonation instability*

The theories of detonation instability summarized in § 4 *a* and § 4 *b* naturally lead to predictions of a regular cell spacing for transverse instabilities in a channel of width W.

The first simple criterion involves the theory of linearized instability for ZND profiles from § 4 *a*. Given the channel width W, consider the family of wavelengths compatible with the channel, i.e. W/j for $j = 1, 2, 3, 4, \ldots$. The predicted cell spacing for the channel with width W is determined by the value W/j with the largest growth rate of linearized instability. This is a theory based on the most unstable linearized wavelength compatible with the geometry. For detonation profiles with a stability diagram similar to the one in figure 6, a recent low-frequency nonlinear asymptotic theory to be reviewed below in § 4 *d* provides support for this prediction for sufficiently narrow channels.

The second class of criteria for cell spacing involves the theories of geometric acoustic instability from § 4 *b*. Thus, we assume that there is a band of translating amplifying transverse acoustic wave patterns so that the conditions in (D) are satisfied for the ZND profile. Associated with each translating amplifying transverse wave pattern in the band is a transverse distance y that this pattern propagates in one reflection cycle. One natural cell-spacing criterion proposed by Majda (1987) is to predict the cell spacing through y^*, the transverse distance travelled in one cycle by the translating wave pattern with the largest amplification rate in unit time. Other possible candidates for the cell spacing predicted by the theory of nonlinear acoustics include $y_{\min}$, the smallest transverse distance travelled in one cycle by any amplifying acoustic wave pattern, and $y_{\max}$, the largest transverse distance travelled in one cycle by any amplifying acoustic wave pattern. The criterion using $y_{\min}$ is similar to the one proposed by Barthel (1974). The above criteria are developed without involving the boundary conditions of the channel width. For a given channel width, W, the same criteria apply among the discrete family of patterns with transverse propagation distance in one cycle given by $y_j = W/j$ for $j = 1, 2, 3, 4, \ldots$.

The ZND profile with stability diagram in figure 7 provides an interesting illustration of the above criteria from nonlinear acoustic instability. For this ZND wave, $y_{\min} = 32, y_{\max} = \infty, y^* = \infty$. The fact that $y^* = \infty$ is readily understood; there is a unique trapped ray pattern which propagates exactly parallel to the detonation front and in this case also has the largest amplification rate. In this example, the criteria of geometric acoustics predict no cells provided the channel width is smaller that 32 and cells equal to the channel width provided that W is larger than 32.

PHILOSOPHICAL TRANSACTIONS OF THE ROYAL SOCIETY A MATHEMATICAL, PHYSICAL & ENGINEERING SCIENCES

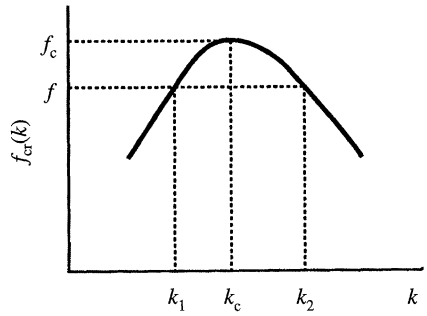

Figure 8. Typical neutral stability curve for low-frequency asymptotic theory.

(*d*) *Low-frequency asymptotic theories for pattern formation in unstable detonations*

Experiments involving unstable detonations exhibit a remarkable number of different unstable patterns involving structures with standing waves (regular cellular transverse structure), travelling waves (spinning detonations), irregular spatio-temporal chaotic patterns (irregular cell structures), and perhaps irregular chaotic fluctuations without cells in certain condensed phases. It is an extremely interesting challenge for the theoreticians interested in detonation physics to develop simpler qualitative–quantitative asymptotic models which might explain at least in a qualitative fashion some of the physical selection mechanisms responsible for discriminating among the various patterns observed. The development of such theories is an ongoing enterprise but nevertheless it is interesting to briefly describe some of the results and current directions. A simple application involving the interaction of such theories and numerical computation in explaining the occurrence of standing waves versus travelling waves will be described in § 5 *d* below.

As in § 3 *d*, the theories use the overdrive, f, as a bifurcation parameter and attempt to mimic theories of nonlinear hydrodynamic stability. The underlying assumption in such asymptotic theories is the existence of a critical overdrive, f_c, so that the neutral stability curve in the linearized stability analysis of the underlying ZND wave has the form depicted in figure 8; as in § 3 *d*, it is assumed that the ZND waves are unstable for overdrives f with $f < f_c$ with the band of unstable wave numbers below the neutral stability curve. Several examples of parameters for ZND waves exhibiting stability curves of this sort are presented by Bourlioux (1991) and Erpenbeck (1970). Also, the asymptotic theories assume spatial periodicity with period W; this is the effective channel width. It is worth mentioning here that other parameters such as the heat release can be used as a bifurcation parameter rather than the overdrive.

(i) *Single travelling mode in a narrow channel*

The requirement of a narrow channel means that given the channel width, W, there is exactly one wave number k^* on the neutral stability curve in figure 8 such that W satisfies $W = (2\pi/k^*)j$ this condition is always satisfied for appropriate narrow channels. Under these circumstances, a simplified asymptotic equation for the nonlinear development of instability can be developed in the same fashion as

described above for one dimension from § 3 *d* (Majda & Roytburd 1993). With

$$\epsilon^2 = f(k^*) - f$$

and $\epsilon \ll 1$, asymptotic solutions of the reactive Euler equations in two space dimensions are constructed with the form

$$\left.\begin{aligned} \psi &= Dt + \epsilon[A(\epsilon^2 t)\exp(\mathrm{i}\omega(k^*, f)t + \mathrm{i}k^* y) + \text{c.c.}] + O(\epsilon^2), \\ u &= u^0(x, f) + \epsilon A(\epsilon^2 t)\boldsymbol{e}(x, k^*, f)\exp(\mathrm{i}\omega(k^*, f)t + \mathrm{i}k^* y) + \text{c.c.} + O(\epsilon^2). \end{aligned}\right\} \tag{4.11}$$

Here and below, $u = {}^t(\rho, \boldsymbol{v}, p, Z)$, ψ defines the perturbed precursor shock front (see (4.1)), c.c. denotes complex conjugate, $\boldsymbol{e}(x, k, f)$ denotes the unstable eigenmode from (4.7) and (4.10) of the linearized stability theory and $\mathrm{i}\omega(k^*, f) = \operatorname{Im}\alpha$ from (4.6). As in equation (3.7), the systematic asymptotic procedure automatically predicts that the amplitude $A(T)$ solves a Landau–Stuart question

$$\frac{\mathrm{d}A}{\mathrm{d}T} = \chi A + \beta A^2 \bar{A}, \tag{4.12}$$

where β, χ are constants determined by the asymptotic procedure with $\chi > 0$, $\operatorname{Re}\beta < 0$. By recalling the analysis from (3.10), (3.11), (3.12) for the equation in (4.14), we see that for narrow channels, since $\omega(k^*, f) \neq 0$ in (4.13), the asymptotic theory predicts that travelling mode solutions arise from travelling mode perturbations of the basic ZND profile in the nonlinear instability process. We will see in § 5 *d* below that such travelling modes are analogues in the small-amplitude regime of structures which resemble spinning detonations.

(ii) *Travelling modes in wide channels*

Here we review the new asymptotic equations that result when many modes of instability compete on wide channels W with $W \gg 1$. We recall from (2.1) that the basic length-scale here is the half-reaction length of the ZND profile so most channel widths in experiments are large. On very wide channels, the sideband instabilities in figure 8 compete to give a partial differential equation for the asymptotic description of pattern formation in the instability process. With $\epsilon^2 = f_c - f$ and $\epsilon \ll 1$ used by Majda & Roytburd (1992), systematic asymptotic solutions of the reactive Euler equations are constructed in the large channel limit, $W = O(\epsilon^{-2})$ by mimicking ideas of nonlinear wave number interaction in hydrodynamic stability theory (Benney & Newell 1967; DiPrima *et al.* 1971; Stewartson & Stuart 1971; Eckhaus & Iooss 1989). These asymptotic solutions have the form

$$\left.\begin{aligned} \psi(y, t) &= D(f)t + \epsilon[A(Y, T)\exp(\mathrm{i}\omega(k_c, f)t + \mathrm{i}k_c y) + \text{c.c.}] + O(\epsilon^2), \\ u(x, y, t) &= u^0(x, f) + \epsilon[A(Y, T)\boldsymbol{e}(x, k_c, f)\exp(\mathrm{i}\omega(k_c, f)t + \mathrm{i}k_c y) + \text{c.c.}] + O(\epsilon^2), \end{aligned}\right\} \tag{4.13}$$

where the arguments of the slow variables Y, T are given by

$$T = \epsilon^2 t, \quad Y = \epsilon(y + \nu t) \tag{4.14}$$

with the wave speed ν given by the group velocity,

$$\nu = \frac{\partial\omega}{\partial k}\Big|_{k=k_c}.$$

asymptotics systematically determine that the amplitude function $A(Y,T)$ satisfies a complex *Ginzburg–Landau* equation,

$$\frac{\partial A}{\partial T} = \chi A + \beta A^2 \bar{A} + \gamma \frac{\partial^2 A}{\partial Y^2}, \tag{4.15}$$

where γ is a complex constant which is computed in the asymptotic procedure while $\chi > 0$ and β with $\operatorname{Re}\beta < 0$ are the same constants as appeared in (4.14) for the narrow channel theory.

The complex Ginzburg–Landau equation is one of the main qualitative model equations describing pattern formation. For various regimes of values of the coefficients χ, β, γ, this equation has many additional stationary, periodic, chaotic (Keefe 1985), and even 'turbulent' (Bartuccelli *et al.* 1990) solutions with behaviour far more complex than that of the simple ODE from (4.14). Because experiments indicate that there is irregular and chaotic behaviour in spatial fluctuations for detonation instability in some physical regimes the occurrence of the complex Ginzburg–Landau equation in the asymptotics suggests a possible qualitative explanation for many of these phenomena. A detailed study of this possibility including the actual values for the coefficients χ, β, γ that can occur in the instability process is currently being pursued by V. Roytburd and the authors.

The following simple examples exhibit that there are many more travelling wave solutions of nonlinear instability on wide channels, W, beyond the simple solutions of the ODE in (4.14) presented in § 3 *d*. The reader can easily verify that the equation in (4.17) has the travelling wave solutions,

$$A = R_N \mathrm{e}^{\mathrm{i}(k_N Y - \omega_N T)}, \tag{4.16}$$

which are spatially periodic on a large channel of width W provided that

$$\left.\begin{aligned} k_N &= \frac{2\pi n}{W}, \quad N = 0, 1, 2, \ldots, \\ R_N^2 &= -\frac{\chi}{(\operatorname{Re}\beta)} + \frac{(\operatorname{Re}\gamma) k_N^2}{(\operatorname{Re}\beta)}, \\ \omega_N &= (\operatorname{Im}\gamma) k_N^2 - (\operatorname{Im}\beta) R_N^2. \end{aligned}\right\} \tag{4.17}$$

Of course the solution with $N = 0$ reduces to the simple narrow channel solution described in (3.11), (3.12) from § 3 *d*.

(iii) *Interaction between standing modes and travelling modes*

We rapidly review the developing asymptotic theory for the interaction of standing waves and travelling waves in the dynamic instability of ZND waves. Here we emphasize the simpler situation involving narrow channels W since we present a simple application later in § 5 *d*.

Standing waves and travelling waves necessarily arise simultaneously as a consequence of the invariance of both the reactive Euler equations and the basic ZND profile to reflection symmetry in the transverse variable y. With $u = {}^t(\rho, v_1, v_2, p, Z)$, this symmetry means that if we define the transformation (Ru) by

$$(Ru)(x,y,t) = {}^t(\rho, v_1, -v_2, p, Z)(x, -y, t), \tag{4.18}$$

then we have the following properties:

(F) (i) If u is a solution of the reacting Euler equations, so is Ru.
(ii) If u_{ZND} is the ZND profile propagating in the x-direction, $Ru_{\mathrm{ZND}} = u_{\mathrm{ZND}}$, i.e. the ZND wave is invariant under R.

The facts in (F) immediately imply the following structure in the linearized stability problem:

(G) If $\boldsymbol{e}(x)\mathrm{e}^{\mathrm{i}ky+\alpha t}$ is an eigenmode of the linearized problem for ZND stability in (4.7) and (4.10), then $(R\boldsymbol{e})(x)\mathrm{e}^{-\mathrm{i}ky+\alpha t}$ is also an eigenmode of the linearized problem in (4.7), (4.10) with the same growth rate.

Clearly linear combination of both of the unstable modes in (G) generate mixtures of amplifying travelling waves or standing waves moving in both transverse directions across the channel. Of course, the fact in (G) means that the stability diagram depicted in figure 8 actually has a second piece centred around $-k_{\mathrm{c}}$ obtained by reflection of figure 8 about the axis. In the case of narrow channels, the asymptotic solutions have the form in (4.13) but the terms of order ϵ, for example, in the shock front perturbation involve the linear superposition,

$$A^{+}(\epsilon^2 t)\exp(\mathrm{i}\omega(k^*, f)t + \mathrm{i}k^* y) + A^{-}(\epsilon^2 t)\exp(\mathrm{i}\omega(k^*, f)t - \mathrm{i}k^* y). \tag{4.19}$$

There is a similar perturbation for u using (G) which we omit. The complex amplitudes $A^{\pm}$ correspond to propagating modes in both directions transverse to the channel and in general these modes interact. As in (4.13), (4.14), the systematic asymptotic procedure yields coupled ODEs for the amplitudes given by

$$\left.\begin{aligned} \frac{\mathrm{d}A^{+}}{\mathrm{d}T} &= \chi A^{+} + \beta|A^{+}|^2 A^{+} + \alpha|A^{-}|^2 A^{+}, \\ \frac{\mathrm{d}A^{-}}{\mathrm{d}T} &= \chi A^{-} + \beta|A^{-}|^2 A^{-} + \alpha|A^{+}|^2 A^{-}, \end{aligned}\right\} \tag{4.20}$$

where $\chi > 0$ and β with $\mathrm{Re}\,\beta < 0$ are the same constants as in (4.14) and α is a complex number calculated in the asymptotic procedure.

The ODEs in (4.24) provide a simplified asymptotic description of the interaction of the two different travelling modes in the dynamic nonlinear transverse instability of the ZND wave. Obviously, the pure travelling mode solutions of § 4 *d* (i) are special solutions of (4.24) with either $A_{+} = 0$ or $A_{-} = 0$. Next we indicate briefly the fashion in which the equations in (4.24) qualitatively determine the preference and selection process of pure travelling modes and standing modes when both effects compete. With the polar coordinates

$$A^{+}(T) = R^{+}(T)\mathrm{e}^{\mathrm{i}\theta_{+}(T)}, \quad A^{-}(T) = R^{-}(T)\mathrm{e}^{\mathrm{i}\theta_{-}(T)},$$

after a simple rescaling of time the ODEs for $R^{\pm}(T)$ become

$$\left.\begin{aligned} \frac{\mathrm{d}R^{+}}{\mathrm{d}T} &= aR^{+} - (R^{+})^3 + b(R^{-})^2 R^{+}, \\ \frac{\mathrm{d}R^{-}}{\mathrm{d}T} &= aR^{-} - (R^{-})^3 + b(R^{+})^2 R^{-}, \end{aligned}\right\} \tag{4.21}$$

where $a > 0$ and b are both real coefficients which are readily computed from χ, β, and α. We omit the equations for the phases, $\theta_{\pm}(T)$, since as in (3.10), these

functions only involve quadrature once $R^{\pm}(T)$ are known. The equations in (4.25) are readily analysed and we summarize their properties below:

(H)
(i) The ZND profile has coordinates $(0,0)$.
(ii) The two travelling waves have coordinates $(R^+,R^-) = (a^{1/2},0),\ (0,a^{1/2})$.
(iii) For $b<1$, the standing wave is a steady solution of (4.25) with coordinates

$$(R^+,R^-)=\left(\left(\frac{a}{1-b}\right)^{1/2},\left(\frac{a}{1-b}\right)^{1/2}\right).$$

The next step is to address which of the four steady states in (H) is actually stable as time evolves for the two ODEs in (4.25). Special perturbations of the form $(R^+(t),0)$ or $(0,R^-(t))$ with $R^+(t)\neq 0$ or $R^-(t)\neq 0$ approach either of the two travelling waves in (H). Similarly, for special symmetric perturbations of the form $(R(t),R(t))$, it is easily verified that provided $R(t)\neq 0$ and $b<1$, these solutions approach the standing wave in (H). Simple arguments using phase plane techniques give the following description of the behaviour for general solutions of (4.25) which do not obey the special symmetries just discussed:

(I)
(i) For $b<-1$, the general solution $(R^+(T),R^-(T))$ of (4.25) approaches one of the two steady travelling waves in (H) as $T\to\infty$; the symmetric mode is unstable dynamically to general perturbations.
(ii) For $b>-1$, both of the travelling modes are unstable dynamically to general perturbations. For $1>b>-1$, the general solution of (4.25) approaches the standing wave solution in (H) as $T\to\infty$. For $b>1$, the general solution of (4.25) has the property that $((R^+)^2+(R^-)^2)(T)$ becomes unbounded as $T\to\infty$ in a symmetric fashion so that $R_+(T)\approx R_-(T)$ for T large.

To summarize, the nonlinear asymptotic theory gives simple conditions depending on the coefficient b in (4.25) so that either travelling modes or standing modes are preferred in the basic process of instability in the ZND wave. The coefficient b can be calculated numerically for any ZND wave with a stability diagram with the form in figure 8. We will describe a simple interaction between the theory just presented and numerical simulations in § 5 *c* (ii).

An asymptotic theory for the interaction of travelling modes and standing modes on channels with large widths, $W\gg 1$, is currently being developed. The simplified asymptotic equations involve two coupled complex Ginzburg–Landau equations as in § 4 *d* (ii) with additional interaction terms that reduce to the simple coupled ODEs in (4.24) in the mean field limiting case. Such equations provide a qualitative model for pattern formation in detonation instability that allows for both regular and irregular transverse wave instabilities as well as mode competition between travelling and standing waves.

Finally, we comment briefly on other work which attempts to model pattern formation for unstable detonations. Erpenbeck (1970) presents nonlinear equations which model the coupling between standing modes and travelling modes on narrow channels by a system of ODEs. Unfortunately Erpenbeck's arguments (Erpenbeck 1966, 1970) suffer from the same defect of deriving non-unique amplitude equations without regard to secular behaviour in the asymptotics as we

PHILOSOPHICAL TRANSACTIONS OF THE ROYAL SOCIETY A MATHEMATICAL, PHYSICAL & ENGINEERING SCIENCES

discussed earlier in the last paragraph of § 3 *d*. In fact, the new asymptotic approach (Majda & Roytburd 1992) eliminates this ambiguity by systematically eliminating secular terms through a unique adjoint problem; furthermore, the result is the system of equations in (4.24) which is much simpler than those derived previously by Erpenbeck.

5. Numerical and theoretical structure for two-dimensional unstable detonations

We begin this section by describing a new numerical method which the authors have developed recently for computing unstable detonations in two space dimensions (Bourlioux 1991; Bourlioux & Majda 1992, 1993). The design principles and validation studies for this code are based on the same considerations which we reviewed in § 3 of this paper for detonation instability in a single space dimension. We include a brief summary of the two-dimensional test problems which we have used in testing this code since this might be of general interest to researchers in computational combustion who are interested in developing improved numerical codes for detonations. Then we review some of the physical insight into detonation instability which has been achieved recently through simulations with this high-resolution method, especially, regarding turbulence in detonations. Finally we summarize the recent comparison of numerical predictions and the theory reviewed in § 4 *c* and § 4 *d* above regarding cell spacing and mode interaction.

(*a*) *A new numerical method for unstable detonations*

Here we present the new numerical method to solve the reactive Euler equations in two space dimensions which we have developed recently and applied to detonation instability. As in a single space variable, the global procedure is a very natural fractional step scheme which involves two ingredients per time step.

In the first fractional step, the hydrodynamics part of the problem is solved; the first three equations in (2.1) are advanced with the reactant mass fraction advected as a passive scalar. In the second fractional step, the species equation is advanced explicitly by integrating the ODE for the mass fraction given the temperature field from the previous fractional step.

The hydrodynamic solver in the first step combines a higher-order Godunov method with conservative front tracking and adaptive mesh refinement. This new solver is designed to meet the following requirements:

(i) sharp and robust representation of the detonation front;

(ii) appropriate representation of all relevant length-scales of the problem, including the small length-scales associated with the stiff chemistry near the front;

(iii) accurate representation of the smooth regions of the flow and accurate, stable capturing of all the other discontinuities behind the leading front.

The higher-order extension of Godunov's method implemented is second-order accurate in space and time, and captures shock waves and other discontinuities with minimal numerical overshoot and dissipation. The method was first introduced by Colella & Woodward (1984). The version used here is a two-dimensional unsplit code as described by Colella (1984).

This scheme is the basic solver for a simplified version of Berger & Colella's (1989) adaptive mesh refinement procedure. To concentrate the computational effort in the region near the front with stiff chemistry, we superimpose on our

PHILOSOPHICAL TRANSACTIONS OF THE ROYAL SOCIETY A MATHEMATICAL, PHYSICAL & ENGINEERING SCIENCES

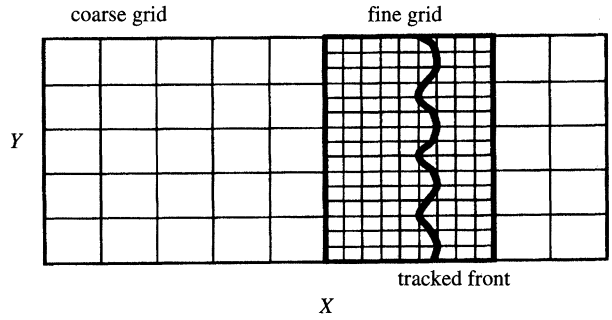

Figure 9. Adaptive grid and front tracking set-up for two-dimensional detonation calculation (detonation moving to the right).

basic uniform grid a rectangular patch of refined grid in the neighbourhood of the leading shock. In the present approach, the width of the fine grid is fixed and the fine grid position is regularly updated along with the entire computational domain to follow the leading shock.

We also implemented the conservative front tracking procedure developed by Chern & Colella (1987). The leading front is represented as a polygonal curve moving through the finite difference mesh and treated as an internal boundary whose motion, along with the fluxes across it, is computed explicitly using Rankine–Hugoniot jump conditions. This procedure avoids the averaging process across the discontinuity as well as the additional numerical viscosity necessary for stable capturing of the shock: the present approach is much more reliable when attempting to compute the physical instability of the discontinuity. We already illustrated this in § 3 in a single space variable.

Unlike typical front tracking or shock-fitting codes, the tracking procedure of Chern & Colella has the advantage that it is fully conservative. This allows the method to capture accurately the other discontinuities behind the tracked leading front. In particular, triple point configurations are computed, where the Mach stem and the incident shock are tracked as parts of the leading front, while the reflected shock and the contact discontinuity, intersecting the leading front from behind, are captured by the finite difference scheme. This procedure has allowed us to compute front instabilities with transverse amplitude too small (a few per cent of the half-reaction length) to be effectively represented by a finite difference grid but that can generate significant perturbations of the flow in their wake for distances of several half-reaction lengths.

(i) *Numerical test suite for code development for two-dimensional detonations*

Here we summarize the test problems which we have used to validate the two-dimensional numerical code which we have just described. This code obviously reduces to the one described in § 3 *c* (ii) in a single space dimension. As described in § 3 of this review, a preliminary 'numerical test suite' for computing one-dimensional unstable detonations was already applied to this numerical code in the first stage of the design procedure. For the two-dimensional numerical code, we used the following four classes of test problems for validation and resolution studies.

(i) Non-reactive test: a shock wave overtaking the tracked leading shock front. An analytic solution is known and this test provides a simple assessment of the capability of the numerical code to treat the interaction of tracked and captured waves with high resolution.

(ii) Non-reactive test: the initial data consists of embedded Mach stems in the conservative tracked front. Without chemical reactions, the physical predictions are decay of the wave pattern to the stable leading shock front. The numerical method had these features in its computed solutions.

(iii) Stable and unstable ZND waves with parameters near stability boundaries: these studies test the capability of the numerical method with realistic mesh spacings to detect stable and unstable wave patterns as predicted by linearized stability theory (see § 4 *a*). Initial data for these tests consisted of perturbing the ZND profile by standing and travelling wave patterns determined by linear theory and also random front perturbations.

(iv) A classical unstable detonation: the instability of the ZND profile with $E^+ = 20, q_0 = 2, f = 1.1$ results in a classical example of the 'explosion within explosion' structure (Urtview & Oppenheim 1966; Lundstrom & Oppenheim 1969; Oppenheim 1985) for propagating regular transverse Mach stems with a very simple structure; the reflected shock waves and vortex sheets are nearly rectilinear and only slightly curved (see figure 10). This example is the simplest case known to the authors for mesh refinement convergence studies for transverse wave structure with Mach stems.

(*b*) *Recent insight into the physical phenomena of unstable detonations*

In the last fifteen years there have been many important contributions to the understanding of unstable detonations through direct numerical simulation of two-dimensional problems. Taki & Fujiwara (1973, 1981) pioneered these efforts and conclusively demonstrated that contemporary numerical methods can reproduce the regular Mach stem cell structure typically observed in experiments with gaseous phases. In their numerical work, Boris, Oran, and their collaborators (Oran *et al.* 1982; Kailasanath *et al.* 1985; Guirguis *et al.* 1986; Boris & Oran 1987) have also demonstrated several other important physical effects in the cellular structure for unstable detonations such as the formation of unreacted gas pockets and also some aspects of irregular cell structures. There are recent simulations of unstable detonations in three dimensions by Schöffel (1989) and Fujiwara & Reddy (1989). Here we describe briefly some of the new physical insights into unstable detonations that have been developed recently through simulations with the numerical code described in § 5 *a*.

(i) *Turbulence in the wake of unstable detonations*

Lee (1988) has suggested that the instability of detonations can be a source of significant turbulence. Recently, by varying the heat release, activation energy, and overdrive, the authors were able to generate the transition to two-dimensional turbulence in the wake of unstable detonations. Furthermore, these numerical computations indicate that in the most unstable cases, the strong turbulence contributes to the irregularity of the cellular pattern. We describe these results and the corresponding physical phenomena briefly below.

In each of figures 10, 11, and 12 we present snapshots of the pressure, temperature, vorticity, and reactant at equal time intervals as three different unstable

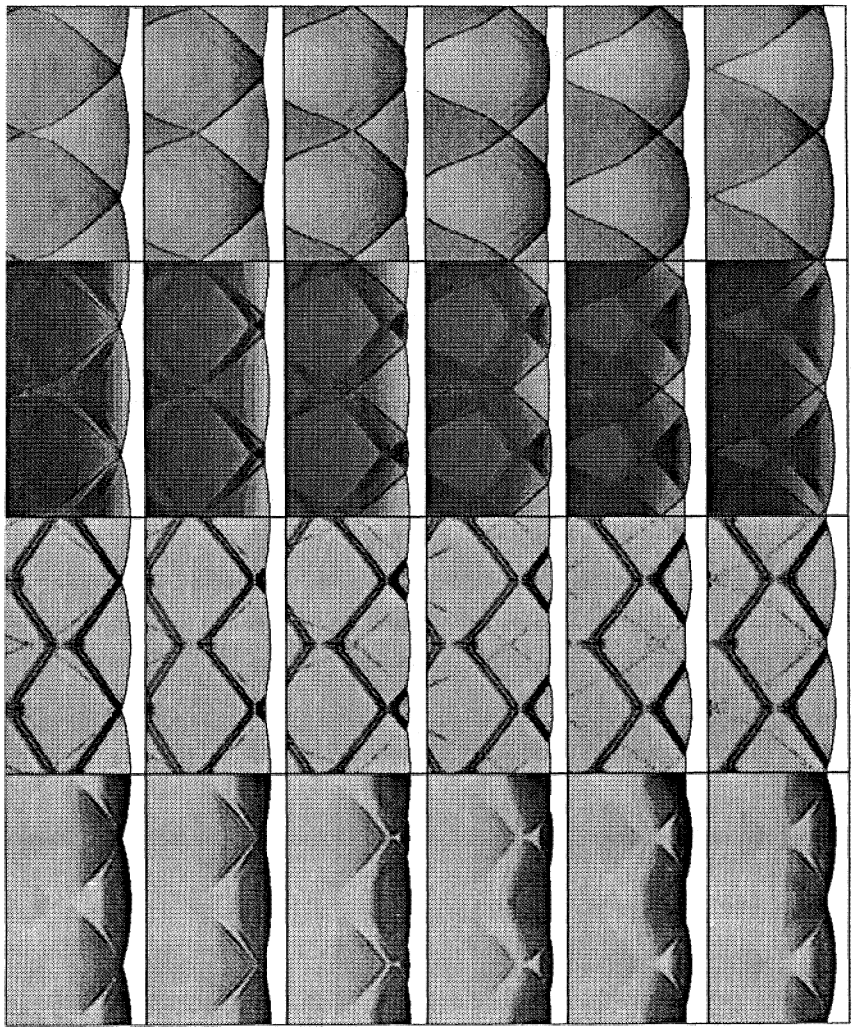

Figure 10. Sequence of six snapshots of the flow field through half a cell cycle (increasing time from left to right, shock moving to the right) with, from top to bottom, pressure, temperature, vorticity and reactant mass fraction. In this sequence and similar sequences to follow, the computational solution is plotted twice vertically for each variable, using the periodic boundary conditions. In the post-shock domain, the grey scale varies linearly between white (minimum) and black (maximum), while the uniform flow field ahead of the shock is always assigned the colour white. $E^+ = 20$; $q_0 = 2$; $f = 1.1$; width is 5.7.

detonations propagate down a channel through one-half a period cycle of the basic transverse wave structure. At the next time interval not displayed the basic structure from the first snapshot is repeated with a phase shift. In figure 10, we plot the transverse instability that emerged from a perturbed ZND profile with $\gamma = 1.2$, $q_0 = 2$, $E^+ = 20$, $f = 1.1$ while for figure 11 the ZND profile had $\gamma = 1.2$, $q_0 = 50$, $E^+ = 10$, and $f = 1.2$; in figure 12, the ZND profile had $\gamma = 1.2$, $q_0 = 50$, $E^+ = 50$ and $f = 1.2$. Thus, the activation energy and heat release increases substantially from figure 10 to figure 11 while the activation energy increases substantially from figure 11 to figure 12 with fixed overdrive and

PHILOSOPHICAL TRANSACTIONS OF THE ROYAL SOCIETY A MATHEMATICAL, PHYSICAL & ENGINEERING SCIENCES

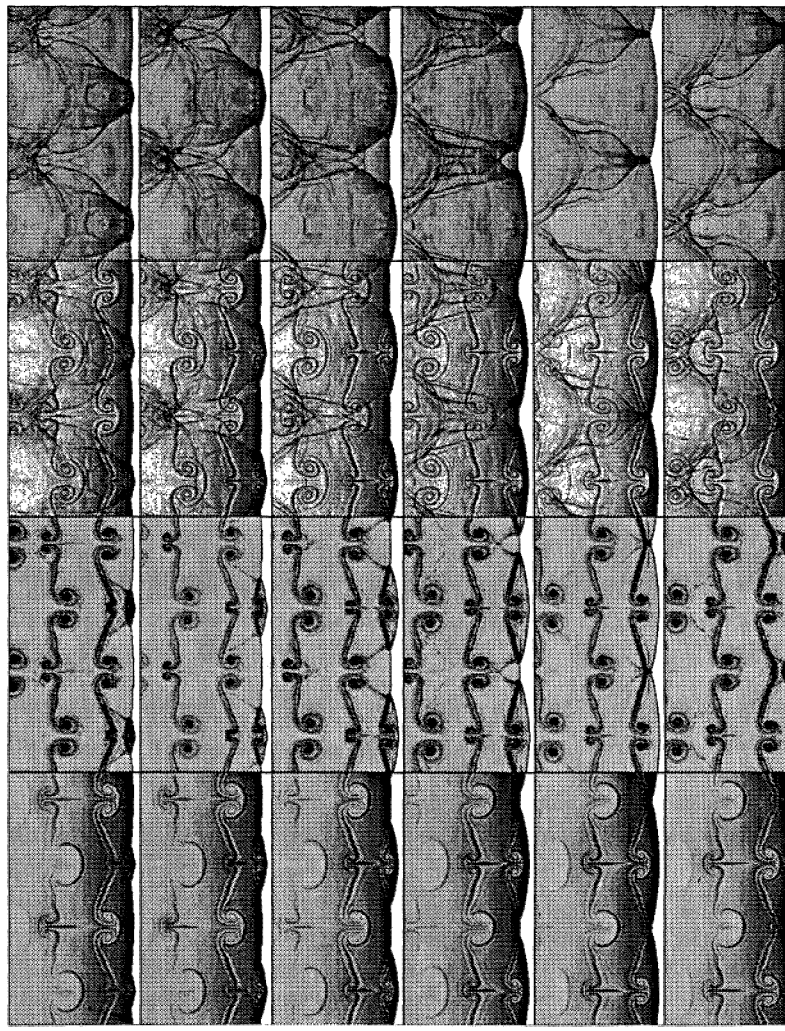

Figure 11. Sequence of six snapshots of the flow field through half a cell cycle (increasing time from left to right, shock moving to the right) with, from top to bottom, pressure, temperature, vorticity and reactant mass fraction. $E^+ = 10$; $q_0 = 50$; $f = 1.2$; width 10 (shown twice).

heat release. A quick glance at the vorticity field displayed in these figures clearly indicates a transition to turbulence with increasing heat release and activation energy. Next we present a brief explanation of these phenomena.

The propagating transverse wave structure in figure 10 confirms the classical picture of 'explosions within explosions' for the propagation of transverse cells in a detonation front (Oppenheim 1972). In the vorticity field from figure 10, the contact discontinuities appear with alternating signs and are nearly straight lines. This picture confirms the classical explanation of the concentrated vortex at the triple point as removing the soot in the physical experiments.

In figure 13, a schematic diagram shows the creation of a new pair of vortex lines of opposite signs at each collision of triple points. In general, when the two new contact discontinuities are formed, the two incoming ones are repelled and drift down the reaction zone. Once they are detached, their tips, which used to be attached to the triple point, will tend to roll up and form two pairs of counter-

PHILOSOPHICAL TRANSACTIONS OF THE ROYAL SOCIETY A MATHEMATICAL, PHYSICAL & ENGINEERING SCIENCES

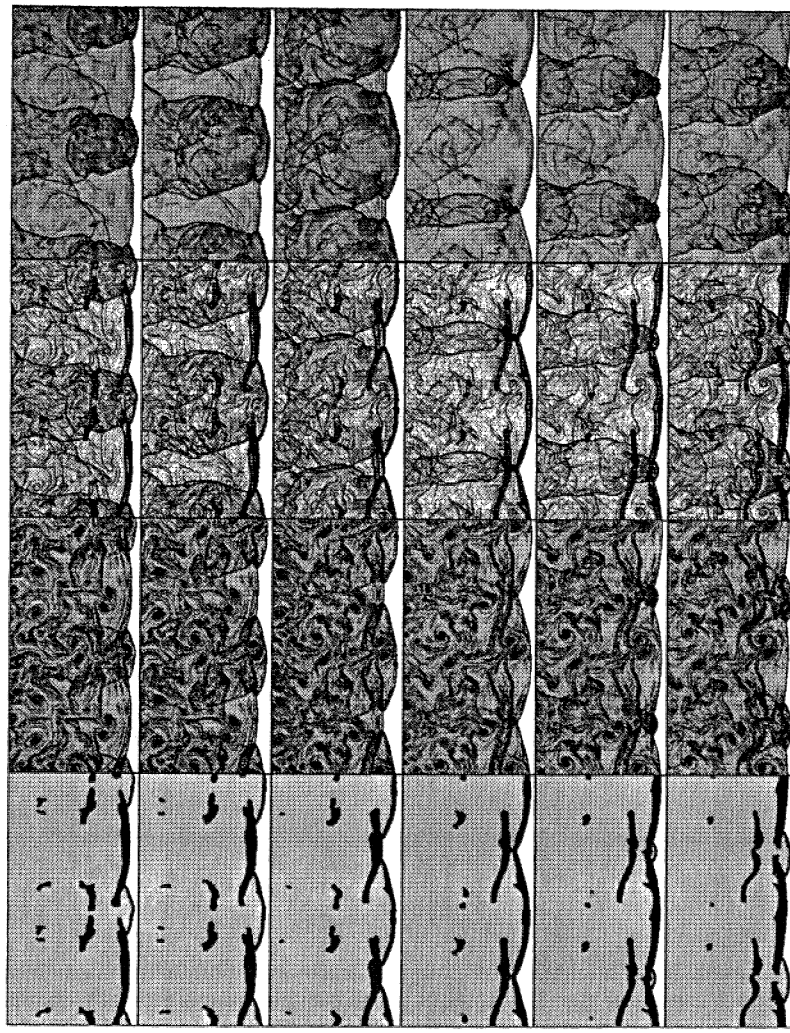

Figure 12. Sequence of six snapshots of the flow field through half a cell cycle (increasing time from left to right, shock moving to the right) with, from top to bottom, pressure, temperature, vorticity and reactant mass fraction. $E^+ = 50$; $q_0 = 50$; $f = 1.2$; width 20 (shown twice).

rotating eddies which repel. This roll up is not visible in figure 10 but the above discussion explains the appearance of the regular coherent plumes in the case graphed in figure 11. Here the heat release is larger and the contact discontinuities have much larger strength so they roll up. Spectacular coherent patterns are observed in the temperature and vorticity fields in figure 11 through the mechanism just outlined above. Next we explain the increased turbulence in the case from figure 12 as compared with the one in figure 11. The transverse waves in figure 12 involve complex structures with multiple trailing Mach configurations which qualitatively resemble those observed in some experiments (Voitsekhovskii *et al.* 1966). The numerical solution displaying this complex structure at one snapshot in time is given in figure 14. Each additional contact discontinuity and curved shock in these multiple trailing configurations provides an additional source of vorticity to generate more turbulence through the basic process depicted in fig-

PHILOSOPHICAL TRANSACTIONS OF THE ROYAL SOCIETY A MATHEMATICAL, PHYSICAL & ENGINEERING SCIENCES

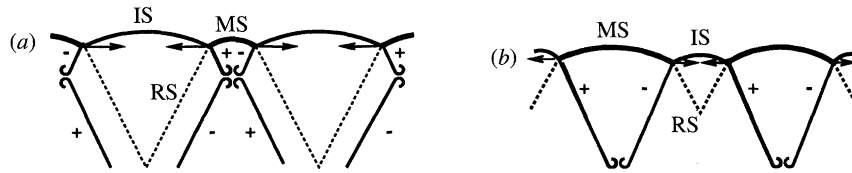

Figure 13. Schematic diagram for collision of triple points and roll-up of vortex sheets, creating pairs of anti-parallel vortices (MS, Mach stem; IS, incident shock; RS, reflected shock; +(−), slip line with positive (negative) vorticity).

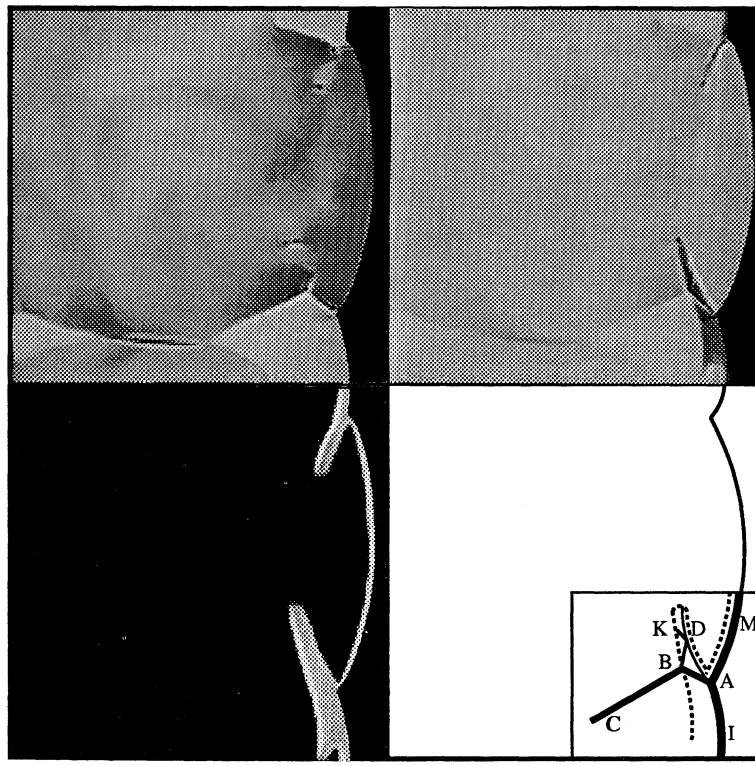

Figure 14. Snapshots of pressure (top left), density (top right), reactant mass fraction (bottom left) along with the corresponding wave diagram (bottom right). The detailed multiple Mach stem structure in the wake of the leading front is in surprising agreement with the experimental results of Voitsekhovskii *et al.* (1966). Following their notation, **M** is the Mach stem, **I** is the incident shock, **A** is the triple point, **AB** is the reflected shock, **B** is also the triple point for the secondary Mach stem configuration, **BC** is the transverse wave segment, **AD** is the slip line, **DK** is part of a centred rarefaction wave. Most of the reaction takes place between the leading shock and the dashed line.

ure 13. On the other hand, the instability in figure 11 is less strong and only involves simple Mach stems: coherent structures strongly dominate the flow field because these additional wave structures are absent. A closer inspection of the vorticity field in figure 12 reveals that the flow field displays many of the features of fully developed two-dimensional turbulence (Brachet *et al.* 1986) in the wake of the detonation front. Also, the numerical front track record for this case indicates that this strong turbulence contributes to the irregularity of the cellular pattern.

PHILOSOPHICAL TRANSACTIONS OF THE ROYAL SOCIETY A MATHEMATICAL, PHYSICAL & ENGINEERING SCIENCES

(ii) *Pattern formation in unstable detonations*

Next, we briefly describe a numerical simulation with strong spatio-temporal irregularity in the cellular structure as time evolves. Since the numerical method tracks the leading precursor shock front, it is natural to display the front track history as a diagnostic. The basic ZND wave from figure 11 has the values $\gamma = 1.2$, $q_0 = 50$, $E^+ = 10$, $f = 1.2$ and the cell spacing in figure 11 computed on a narrow channel is 10. This ZND wave is an interesting example with several competing modes of instability with comparable growth rates. In figure 15 we present the front track history for a numerical simulation on a wider channel with $W = 40$. Clearly, the front track history displays irregular cells in space-time with a qualitative structure which strongly resembles the irregular cells in the classical experiments of Strehlow (1978). As discussed in § 4 *d*, coupled complex Ginzburg–Landau equations are capable of producing similar chaotic phenomena in appropriate regimes of the coefficient values. Since current asymptotic theories establish a link between these equations and detonation instability, the qualitative resemblance in the corresponding solutions may not be entirely coincidental.

(*c*) *Comparison of theory and numerics*

Here we briefly discuss the comparison between the qualitative and quantitative theoretical predictions for cell spacing and mode interaction described in § 4 *c* and § 4 *d* above with the results of high-resolution numerical simulations designed specifically to test these theories.

(i) *Theoretical and numerical predictions for cell spacing*

Eight numerical experiments were developed by the authors (Bourlioux & Majda 1992) which systematically tested the two theories for cell spacing which we summarized in § 4 *c*. Four of the ZND profiles were stable at short wavelengths and had simple stability diagrams like the one in figure 6. The other four cases involved ZND profiles that were unstable at short wavelengths with complex instability diagrams as depicted in figure 7.

First, we discuss the simplest theory for cell spacing based on the most unstable linearized wavelength for the ZND profile. This theory gave a remarkably accurate prediction for the cell spacing for four of the ZND profiles provided the channels had a sufficiently narrow width. These were the four cases characterized by the fact that the ZND profile is stable at high wave numbers and has a simple finite band of unstable modes at long wavelengths as in figure 6. Two of these examples have the cellular structures which we discussed earlier in figures 10 and 11. In one of the four cases corresponding to the case in figure 11 with stability diagram in figure 6, the simple predictions of cell spacing via linear theory are only qualitatively relevant: for a given channel width, the cell spacing is not necessarily unique with a dependence on the characteristic wavelengths in the initial data and nonlinear mode competition among several modes with comparable growth rates. These aspects are discussed further in § 5 *c* (iii). Furthermore, the four cases where the ZND profile is unstable at short wavelengths illustrate that the simple theory based on most unstable linearized wavelengths can fail when there is a more complex stability diagram. The example in figure 12 with the complex stability diagram in figure 7 illustrates this point dramatically. When ZND profiles are unstable at short wavelengths, there is an enormous range of

PHILOSOPHICAL TRANSACTIONS OF THE ROYAL SOCIETY A MATHEMATICAL, PHYSICAL & ENGINEERING SCIENCES

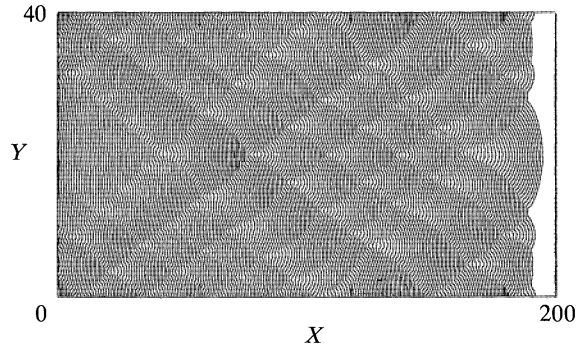

Figure 15. Front track: irregular cellular pattern; $E^+ = 50$; $q_0 = 10$; $f = 1.2$; width is 40.

unstable wavelengths in the ZND profile with comparable growth rates and any noise excites many instabilities rather than selecting a preferred mode.

Next we discuss the comparison between numerical simulations and cell spacings based on the theory of geometric acoustics summarized in § 4 *b* and § 4 *c*. The first naive expectation based on the theory of geometric acoustics is that the two conditions in (D) need to be satisfied in order for transverse Mach stems to form in detonation instability from a ZND wave. Two counter-examples are depicted in figures 10 and 11. The ZND profile in figure 1 is type D so that by the criterion in (E), no rays are trapped so that the two conditions in (D) are violated in dramatic fashion; nevertheless, as given in figure 10, the development of instability in this wave leads to transverse Mach stems. Similarly, the detonation wave with stability diagram in figure 6 has type M so that there are trapped rays but none of these waves amplify so that the conditions in (D) are violated; again, figure 11 indicates that transverse Mach stems develop for this case. For the four ZND waves that are unstable at short wavelengths used in the numerical computations, the theory of geometric acoustics predicts cell spacings as described in § 4 *c* that, respectively, differ by two orders of magnitude, or are 2 or 3/2 times as large, or agree with the numerically computed cell spacing. All three of the examples with relatively good agreement between geometric acoustics and the numerical simulations for cell spacing are very unstable ZND waves with large growth rates. The numerical computations give no evidence for the specific mechanisms of nonlinear acoustics summarized in § 4 *b*; because there are large growth rates at all wave numbers for these ZND waves, large amplitude effects rapidly dominate the basic process of instability so any agreement might be fortuitous.

(ii) *Mode interaction in unstable detonations*

The cellular mode of instability and spinning detonations are examples of large-amplitude standing waves and travelling waves which arise in unstable detonations. The asymptotic theory at small amplitudes discussed in § 4 *d* (iii) and summarized in (4.27) suggests that either standing waves or travelling waves of instability can emerge from the instability of ZND waves under appropriate circumstances. Here we present the results of numerical computations which confirm that both possibilities described in (4.27) actually occur.

Since the numerical method from § 5 *a* computes the leading shock front as a polygonal curve, it is natural to plot the maximum and minimum amplitudes of

PHILOSOPHICAL TRANSACTIONS OF THE ROYAL SOCIETY A MATHEMATICAL, PHYSICAL & ENGINEERING SCIENCES

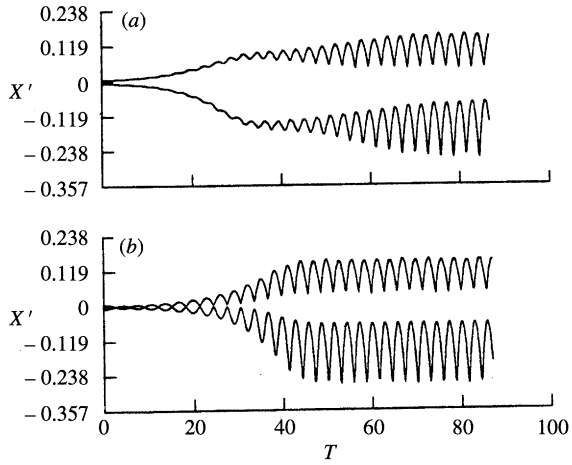

Figure 16. Front perturbation amplitude min–max history for $\gamma = 1.2$, $q_0 = 2$, $E^+ = 20$, and $f = 1.1$: (*a*) travelling wave initial data; (*b*) standing wave initial data.

the perturbed front as time evolves; we call this diagnostic the front perturbation amplitude min–max history. In figure 16 we present the front min–max history for two initial perturbations of the ZND wave with profile in figure 1 with $\gamma = 1.2$, $q_0 = 2$, $E^+ = 20$, and $f = 1.1$. In figure 16*a*, the initial data was the ZND profile perturbed slightly by an unstable travelling mode with the most unstable wavelength of linearized stability theory, while in figure 16*b* we used standing wave perturbations with the same features. For times T with $T > 70$, both front min–max histories have the same oscillatory structure characteristic of a standing wave. In fact at these times, the actual solution has the transverse wave structure which we depicted earlier in figure 10. In this example, travelling modes are unstable and standing modes are stable.

Next we present numerical results which illustrate the opposite behaviour predicted by (4.27). In figure 17 we give the front min–max history for travelling and standing wave perturbations of a ZND profile with $\gamma = 3$, $q_0 = 0.125$, $E^+ = 50$, $f = 1.2$. In this case the graphs in figure 17 indicate that both the standing wave and travelling wave initial data evolve to a travelling wave by the times $T \approx 50$. It is amusing to look at a snapshot of the resulting travelling wave that emerges in both calculations which is presented in figure 18. The result is a strong transverse propagating travelling wave where all the combustion occurs in a localized fashion. This type of structure is very similar to the marginal 'spinning' detonations sometimes observed in round tubes (Fickett & Davis 1979); however, in this case the heat release is apparently too small to generate transverse discontinuities and sustain a fully fledged triple point configuration. This calculation confirms the second theoretical possibility in (4.27) where the travelling modes are both stable but the symmetric standing mode is dynamically unstable.

Another interesting type of mode interaction occurs when the given ZND profile has several competing modes of linearized instability of comparable growth rate for a given channel width. The ZND wave with the parameters $E^+ = 10$, $q_0 = 50$, and $f = 1.2$ on a channel of width $W = 40$ is an example satisfying these conditions. There are three modes of linearized instability for the ZND profile

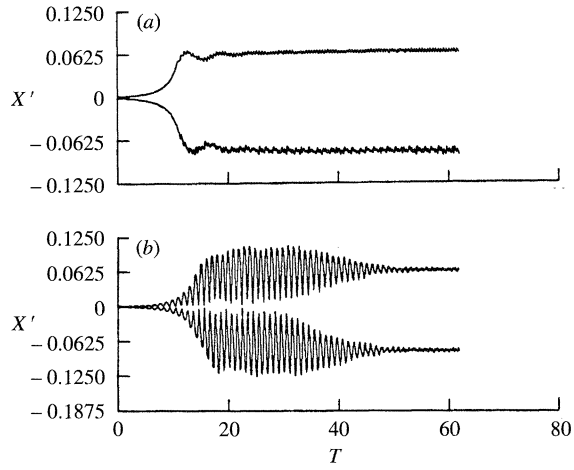

Figure 17. Front perturbation amplitude min–max history for $\gamma = 3$, $q_0 = 0.125$, $E^+ = 50$, and $f = 1.2$: (a) travelling wave initial data; (b) standing wave initial data.

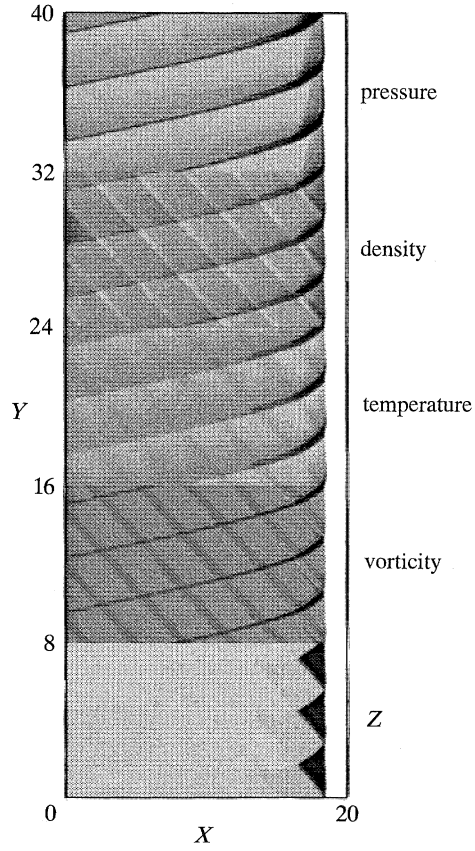

Figure 18. Snapshot of the flow field; shock moving down and to the right. $\gamma = 3$, $q_0 = 0.125$, $E^+ = 50$, and $f = 1.2$ (black, maximum; white, minimum).

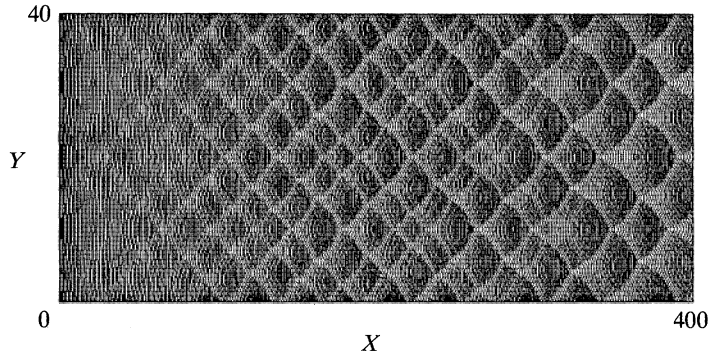

Figure 19. Front track: competition between modes 4 and 6. $E^+ = 50$; $q_0 = 10$; $f = 1.2$; width is 40.

with nearly comparable largest growth rates and compatible with the channel width, $W = 40$. These modes of linearized instability predict cell spacings of 4, 6, 8, i.e. have wavelengths $W = 10, 40/6, 5$, with comparable and largest linearized growth rates given respectively by $\mathrm{Re}\,(\alpha) = 0.19, 0.22, 0.21$. The reader can confirm these approximate values by looking back at figure 6. To illustrate the nonlinear mode competition in this example, we perturbed the ZND profile by a combination of the modes with wavelength $W = 10$ and $W = 40/6$ with equal and very small amplitudes. We display the front track history in figure 19. As the reader can see, both modes interact nonlinearly for a long time; however, ultimately a nonlinear pattern with four cells across the channel emerges. A similar outcome was observed when the linearized modes with spacings 4 and 8 were excited initially with equal amplitudes.

According to linear theory both of the modes with cell spacing $6, 8$ have larger growth rates than the mode with cell spacing 4. Nevertheless mode 4 emerges from the nonlinear competition. This example shows that the simple theoretical predictions of cell spacing described in § 4 *c* based upon the most unstable linearized wave compatible with a given channel width are only qualitatively relevant and nonlinear mode interaction can dominate even for detonations with a very simple instability diagram as in figure 6. It is also worth mentioning that in this example, the cell spacing depends on the initial data. If a pure mode of instability with mode $4, 6$, or 8 and small amplitude was superimposed initially on the ZND profile, regular cells with spacing $4, 6$, and 8 were observed throughout the calculation even at the largest amplitudes. Thus, the cell spacing is not necessarily unique on a given channel even though the unperturbed ZND profile has a very simple stability diagram.

To further emphasize all of these points, we note that figures 15 and 19 involve respectively random and systematic multi-mode initial perturbations of the same ZND profile for a channel with $W = 40$. Also figure 11 involves perturbations of the same ZND profile for a channel with $W = 20$. The characteristic cell sizes that emerged from the numerical simulations in all of these cases had sizes between 8 and 11. This is similar to the behaviour in actual experiments where a nearly characteristic cell size often emerges on sufficiently wide channels. Nevertheless our numerical experiments with an appropriate pure single mode of instability

for the initial data indicate that other nonlinear cells with other spacings are possible and are dynamically stable.

6. Concluding remarks

In this review, we have stressed the symbiotic interaction between asymptotic and numerical ideas in simpler models in improving our understanding of the physical phenomena of unstable detonations. An obvious direction for future research is to assess the effects of more complex and realistic chemistry models on the theories for detonation instability and to design numerical codes to deal efficiently with them.

The authors thank their collaborators and friends, Victor Roytburd and Phil Colella, for generously sharing their scientific insights with us, both through the past several years and explicitly in this review. They also express their gratitude to Anthony Oppenheim for his constructive comments during the preparation of this manuscript. A.B. is a fellow of the Miller Research Institute at the University of California, Berkeley. The research work of A.J.M. was partly supported by grants A.R.O. DAAL03-92-G-0010, O.N.R. N00014-89–J-1044, and N.S.F. DMS-9001805. The numerical calculations in this paper were performed on the CRAY-YMP at the Pittsburgh National Supercomputer Center funded by the National Science Foundation.

References

Abouseif, G. E. & Toong, T. Y. 1982 Theory of unstable one-dimensional detonations. *Combust. Flame* **45**, 67–94.

Barthel, H. O. 1974 Predicted spacings in hydrogen–oxygen–argon detonations. *Phys. Fluids* **17**, 1547–1907.

Barthel, H. O. & Strehlow, R. A. 1966 Wave propagation in one-dimensional reactive flows. *Phys. Fluids* **9**, 1896–1907.

Bartucceli, M., Constantin, P., Doering, C., Gibbon, J. & Giffelfault, M. 1990 On the possibility of soft and hard turbulence in the Ginzburg–Landau equation. *Physica* D **44**, 421–444.

Berger, M. & Colella, P. 1989 Local adaptive mesh refinement for shock hydrodynamics. *J. Comp. Phys.* **82**, 64–84.

Ben-Artzi, M. 1989 The generalized Riemann problem for reactive flows. *J. Comp. Phys.* **81**, 70–101.

Benney, D. J. & Newell, A. C. 1967 Propagation of nonlinear wave envelopes. *Stud. appl. Math.* **46**, 133–139.

Boris, J. P. & Book, D. L. 1973 Flux corrected transport. I. SHASTA. *J. Comp. Phys.* **23**, 38–69.

Boris, J. P. & Oran, E. S. 1987 *Numerical simulation of reactive flow.* New York: Elsevier.

Bourlioux, A. 1991 Numerical study of unstable detonations. Ph. D. thesis, Program in Applied and Computational Mathematics, Princeton University.

Bourlioux, A. & Majda, A. 1992 Theoretical and numerical structure for unstable two dimensional detonations. *Combust. Flame* **90**, 211–229.

Bourlioux, A. & Majda, A. 1993 High resolution numerical simulations for two-dimensional unstable detonations. *Acta. Astr. Proc. 13th ICDERS Meeting*, Nagoya Japan.

Bourlioux, A., Majda, A. & Roytburd, V. 1991*a* Theoretical and numerical structure for unstable one-dimensional detonations. *SIAM J. appl. Math.* **51**, 303–343.

Bourlioux, A., Majda, A. & Roytburd, V. 1991*b* Nonlinear development of low frequency one-dimensional instabilities for reacting shocks. In *Dynamic issues in combustion* (ed. P. Fife, A. Linan & F. Williams), vol. 35, pp. 63–83. IMA volumes in Mathematics and its Applications. New York: Springer-Verlag.

Brachet, M., Meneguzzi, M. & Sulem, P. 1986 Small-scale dynamics of high Reynolds number two-dimensional turbulence. *Phys. Rev. Lett.* **57**, 683–686.

PHILOSOPHICAL TRANSACTIONS OF THE ROYAL SOCIETY A MATHEMATICAL, PHYSICAL & ENGINEERING SCIENCES

Bukiet, B. 1987 Ph. D. thesis, Courant Institute of Mathematical Sciences, New York University, New York.

Chern, I. & Colella, P. 1987 A conservative front tracking method for hyperbolic conservation laws. Preprint UCRL-97200, Lawrence Livermore National Laboratory.

Chorin, A. J. 1976 Random choice solution of hyperbolic systems. *J. Comp. Phys.* **22**, 517–531.

Colella, P. 1984 A multidimensional second-order Godunov scheme for conservation laws. Preprint LBL-17023, Lawrence Berkeley Laboratory.

Colella, P., Majda, A. & Roytburd, V. 1986 Theoretical and numerical structure for reacting shock waves. *SIAM J. Sci. statist. Comput.* **7**, 1059–1080.

Colella, P. & Woodward, P. 1984 The piecewise parabolic method (PPM) for gas-dynamical simulations. *J. Comp. Phys.* **54**, 174–201.

DiPrima, R., Eckhaus, W. & Segel, L. 1971 Nonlinear wave-number interaction in near-critical two-dimensional flows. *J. Fluid Mech.* **49**, 705–744.

Drazin, P. & Reid, W. 1981 *Hydrodynamic stability*, ch. 7. Cambridge University Press.

Eckhaus, W. & Iooss, G. 1989 Strong selection or rejection of spatially periodic patterns in degenerate bifurcations. *Physica* D **39**, 124–146.

Erpenbeck, J. J. 1962 Stability of steady-state equilibrium detonations. *Phys. Fluids* **5**, 604–614.

Erpenbeck, J. J. 1964 Stability of idealized on-reaction detonations. *Phys. Fluids* **7**, 684–696.

Erpenbeck, J. J. 1966 Detonation stability for disturbances of small transverse wavelength. *Phys. Fluids* **9**, 1293–1306

Erpenbeck, J. J. 1969 Theory of detonation stability. In *Twelfth symposium (international) on combustion*, Pittsburgh: The Combustion Institute, 711–721.

Erpenbeck, J. J. 1970 Nonlinear theory of two-dimensional detonations. *Phys. Fluids* **13**, 2007–2026.

Fickett, W. & Davis, W. C. 1979 *Detonation.* Berkeley: University of California Press.

Fickett, W. & Wood, W. W. 1966 Flow calculation for pulsating one-dimensional detonation. *Phys. Fluids* **9**, 903–916.

Fujiwara, T. & Reddy, K. 1994 Propagation mechanism of detonation: three dimensional phenomena. In *Proc. 12th ICDERS Meeting, Progress in Astronautics and Aeronautics Series.* (In the press.)

Godunov, S. K. 1959 Difference methods for the numerical calculations of discontinuous solutions of the equations of fluid dynamics. *Math. Sb.* **47**, 271–306.

Guirguis, R., Oran, E. S. & Kailasanath, K. 1986 Numerical simulation of the cellular structure of detonations in liquid nitromethane – regularity of the cell structure. *Combust. Flame* **65**, 339–365.

Harten, A., Osher, S., Engquist, B. & Chakravarthy, S. R. 1987 Uniformly high order accurate essentially non-oscillatory schemes. *J. Comp. Phys.* **71**, 231–247.

Kailasanath, K., Oran, E. S., Boris, J. P. & Young, T. R. 1985 Determination of detonation cell size and the role of transverse waves in two-dimensional detonations. *Combust. Flame* **61**, 199–209.

Keefe, L. R. 1985 Dynamics of perturbed wavetrain solutions to the Ginzburg–Landau equation. *Stud. appl. Math.* **73**, 91–153.

Lee, H. I. & Stewart, D. S. 1990 Calculation of linear detonation instability. I. One-dimensional instability of plane detonation. *J. Fluid Mech.* **216**, 103–132.

Lee, J. H. S. 1988 On the universal role of turbulence in the propagation of deflagrations and detonations. In *Computational fluid mechanics and reacting gas flows* (ed. B. Engquist *et al.*), vol. 12, pp. 169–193. IMA Volumes in Mathematics and its Applications.

LeVeque, R. J. & Yee, H. C. 1990 A study of numerical methods for hyperbolic conservation laws with stiff source terms. *J. Comp. Phys.* **86**, 187–210.

Lundstrom, E. A. & Oppenheim, A. K. 1969 On the influence of non-steadiness on the thickness of the detonation wave. *Proc. R. Soc. Lond.* A **310**, 463–478.

Mader, C. L. 1979 *Numerical modeling of detonations.* Berkeley: University of California Press.

PHILOSOPHICAL TRANSACTIONS OF THE ROYAL SOCIETY A MATHEMATICAL, PHYSICAL & ENGINEERING SCIENCES

Majda, A. 1981 A qualitative model for dynamic combustion. *SIAM J. appl. Math.* **41**, 70–93.

Majda, A. 1986 High Mach number combustion. In *Reacting flows: combustion and chemical reactors*. AMS Lectures in Applied Mathematics, vol. 24, pp. 109–184.

Majda, A. 1987 Criteria for regular spacing of reacting Mach stems. *Proc. natn. Acad. Sci. USA* **84**, 6011–6014.

Majda, A. & Roytburd, V. 1988 Numerical modeling of the initiation of reacting shock waves. In *Computational fluid mechanics and reacting gas flows* (ed. B. Engquist *et al.*). IMA Volumes in Mathematics and its Applications, vol. 12, pp. 195–217. New York: Springer-Verlag.

Majda, A. & Roytburd, V. 1990 Numerical study of the mechanisms for initiation of reacting shock waves. *SIAM J. Sci. statist. Comp.* **11**, 950–974.

Majda, A. & Roytburd, V. 1992 Low frequency multidimensional instabilities for reacting shock waves. *Stud. appl. Math.* **87**, 135–174.

Majda, A. & Roytburd, V. 1993 Asymptotic equations for pattern formation in unstable detonations. (In preparation.)

Moen, I. O., Funk, J. W., Ward, S. A., Rude, G. M. & Thibault, P. A. 1984 Detonation length scales for fuel–air explosives. *Prog. Aeronaut. Astronautics* **94**, 55–79.

Oppenheim, A. K. 1972 *Introduction to gasdynamics of explosions*. Courses and Lectures no. 48 of the International Center for Mechanical Sciences, Udine. New York: Springer-Verlag.

Oppenheim, A. K. 1985 Dynamic features of combustion. *Phil. Trans. R. Soc. Lond.* A **315**, 471–508.

Oran, E. & Boris, J. P. 1987 *Numerical simulation of reactive flow*. New York: Elsevier.

Oran, E. S., Young, T. R., Boris, J. P., Picone, J. M. & Edwards, D. H. 1982 A study of detonation structure: the formation of unreacted gas pockets. In *Nineteenth Symp. (Int.) on Combustion*, pp. 573–582. The Combustion Institute.

Rosales, R. & Majda, A. 1983 Weakly nonlinear detonation waves. *SIAM J. appl. Math.* **43**, 1086–1118.

Schöffel, S. The mechanism of spinning detonation – numerical study for a rectangular cross-section tube. In *Proc. 12th ICDERS Meeting, Progress in Astronautics and Aeronautics Series*. (In the press.)

Stewartson, K. & Stuart, J. T. 1971 A nonlinear instability for a wave system in plane Poiseuille flow. *J. Fluid Mech.* **48**, 529–546.

Strehlow, R. A. 1978 *Fundamentals of combustion*. Huntington, New York: Kreiger Publishing.

Strehlow, R. A. & Fernandes, F. D. 1965 Transverse waves in detonations. *Combust. Flame* **9**, 31–58.

Sweeby, P. K. 1984 High resolution schemes using flux limiters for hyperbolic conservation laws. *SIAM J. numer. Analysis* **21**, 995–1011.

Taki, S. & Fujiwara, T. 1973 Numerical analysis of two-dimensional nonsteady detonations. *AIAA J.* **16**, 73–85.

Taki, S. & Fujiwara, T. 1981 Numerical simulation of triple shock behavior of gaseous detonations. In *Eighteenth Symp. (Int.) on Combustion*, pp. 1641–1649 The Combustion Institute.

Urtview, P. E. & Oppenheim, A. K. 1966 Experimental observations of the transition to detonation in an explosive gas. *Proc. R. Soc. Lond.* A **295**, 13–28.

Voitsekhovskii, B. V., Mitrofanov, V. V. & Topchian, M. E. 1966 Structure of a detonation front in gases. Novosibirsk: IZD-VO Sibirsk, Otdel. Adad. Nauk SSST 1963, translation: Wright–Patterson Air Force Base Report FTD-MT 64–257.

Received 19 February 1993; accepted 17 May 1993

PHILOSOPHICAL TRANSACTIONS OF THE ROYAL SOCIETY A MATHEMATICAL, PHYSICAL & ENGINEERING SCIENCES

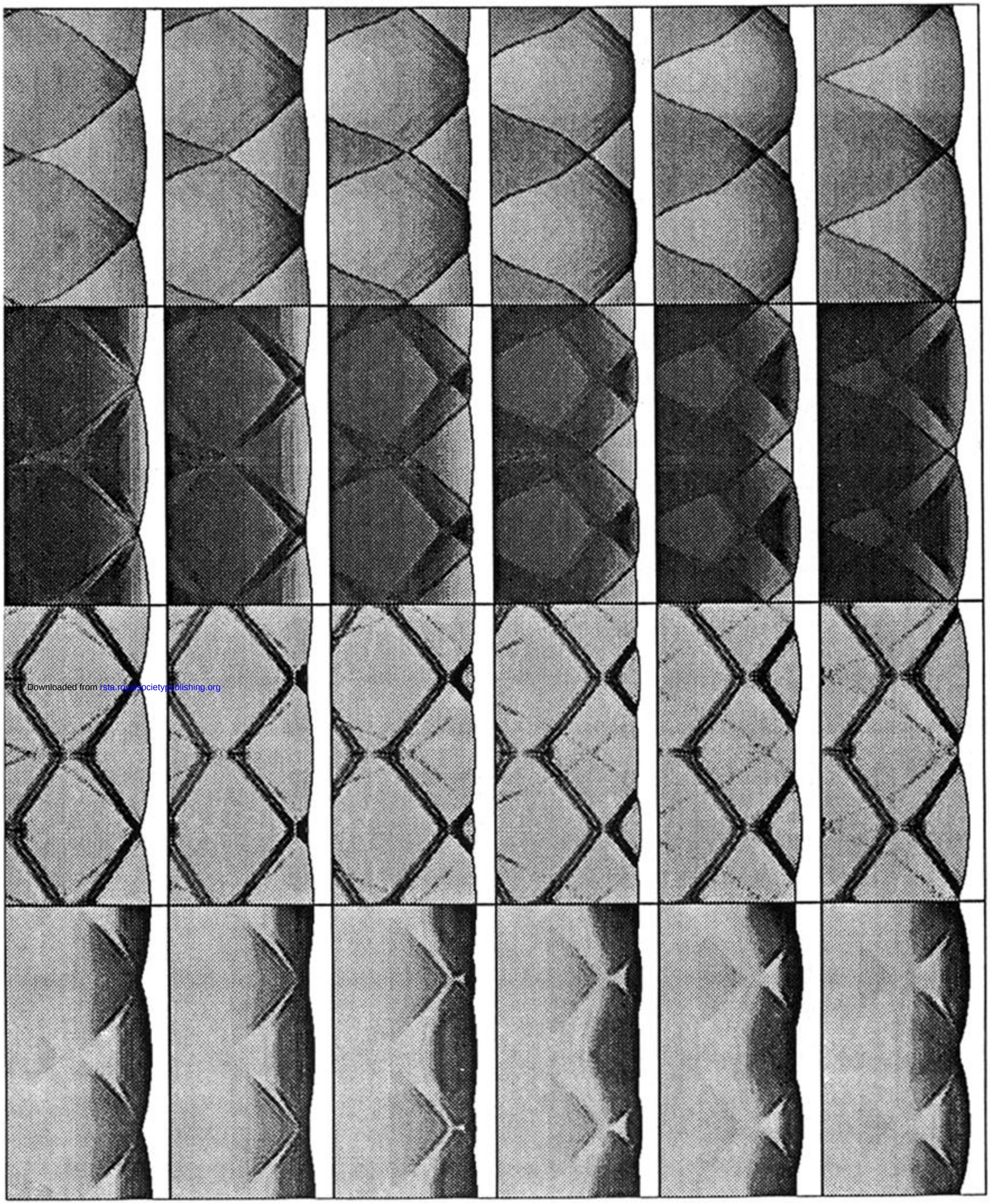

igure 10. Sequence of six snapshots of the flow field through half a cell cycle (increasing time om left to right, shock moving to the right) with, from top to bottom, pressure, tempera- ire, vorticity and reactant mass fraction. In this sequence and similar sequences to follow, the mputational solution is plotted twice vertically for each variable, using the periodic boundary nditions. In the post-shock domain, the grey scale varies linearly between white (minimum) d black (maximum), while the uniform flow field ahead of the shock is always assigned the lour white. $E^+ = 20$; $q_0 = 2$; $f = 1.1$; width is 5.7.

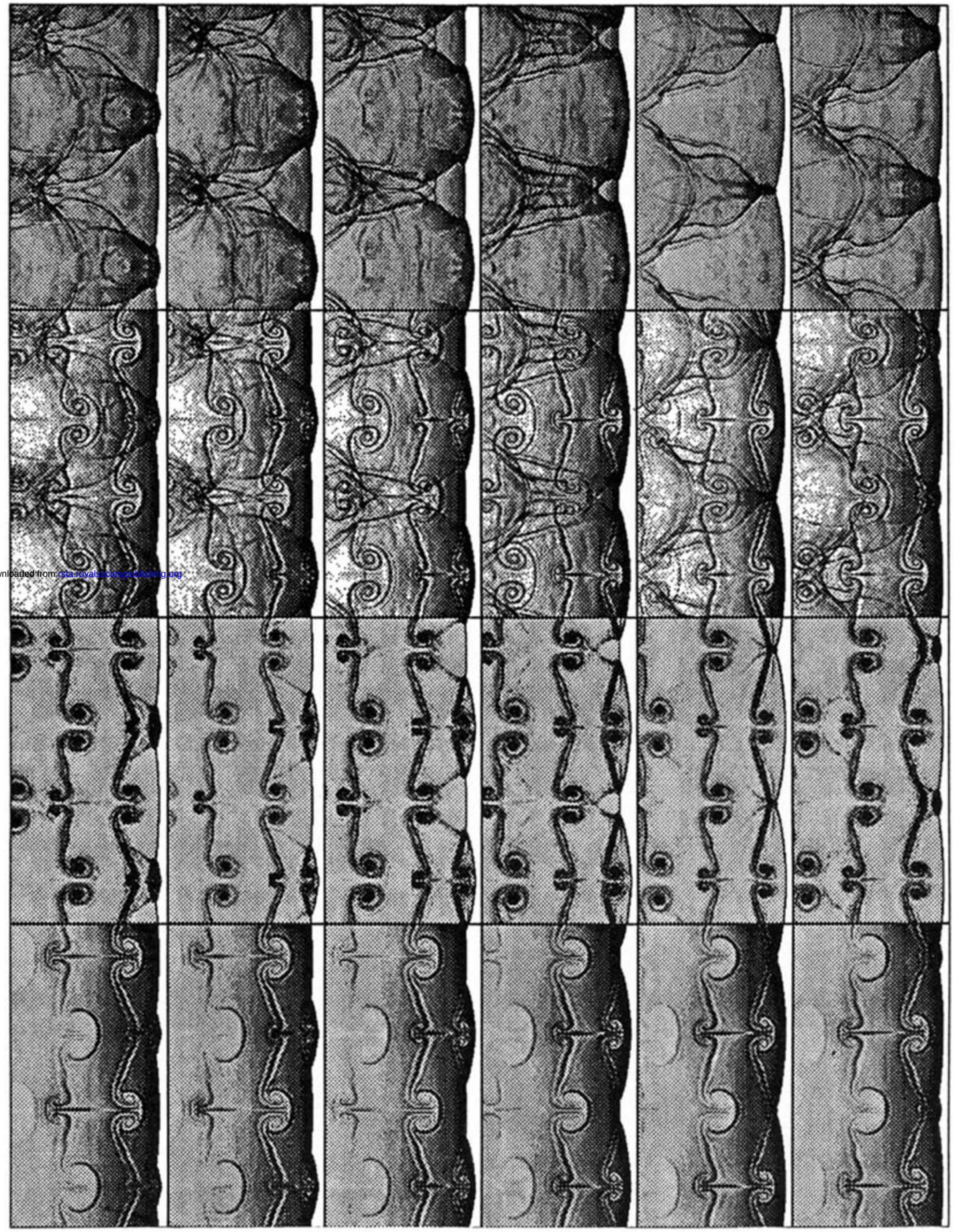

PHILOSOPHICAL TRANSACTIONS OF THE ROYAL SOCIETY A MATHEMATICAL, PHYSICAL & ENGINEERING SCIENCES

'igure 11. Sequence of six snapshots of the flow field through half a cell cycle (increasing time 'rom left to right, shock moving to the right) with, from top to bottom, pressure, temperature, orticity and reactant mass fraction. $E^+ = 10$; $q_0 = 50$; $f = 1.2$; width 10 (shown twice).

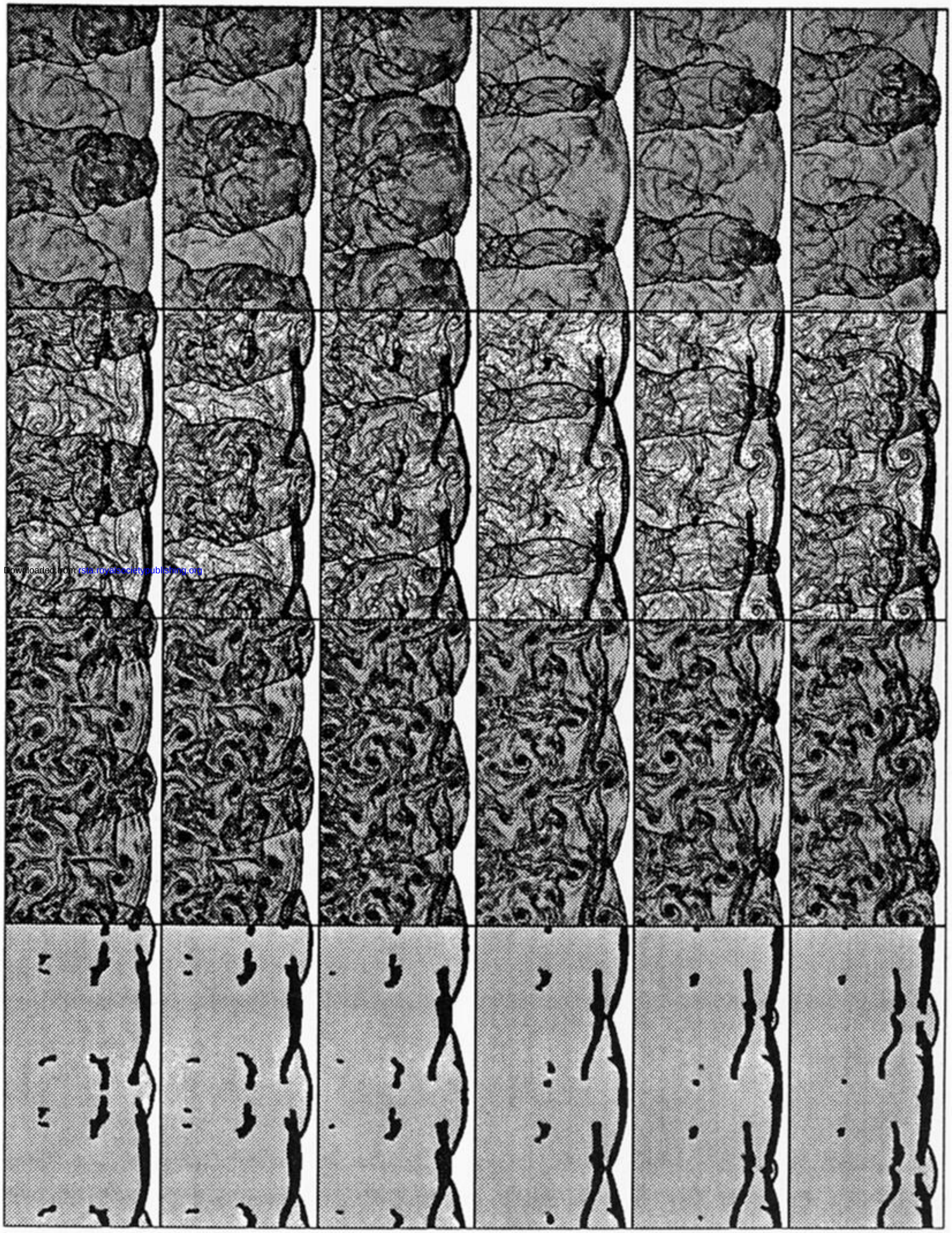

Figure 12. Sequence of six snapshots of the flow field through half a cell cycle (increasing time from left to right, shock moving to the right) with, from top to bottom, pressure, temperature, vorticity and reactant mass fraction. $E^+ = 50$; $q_0 = 50$; $f = 1.2$; width 20 (shown twice).

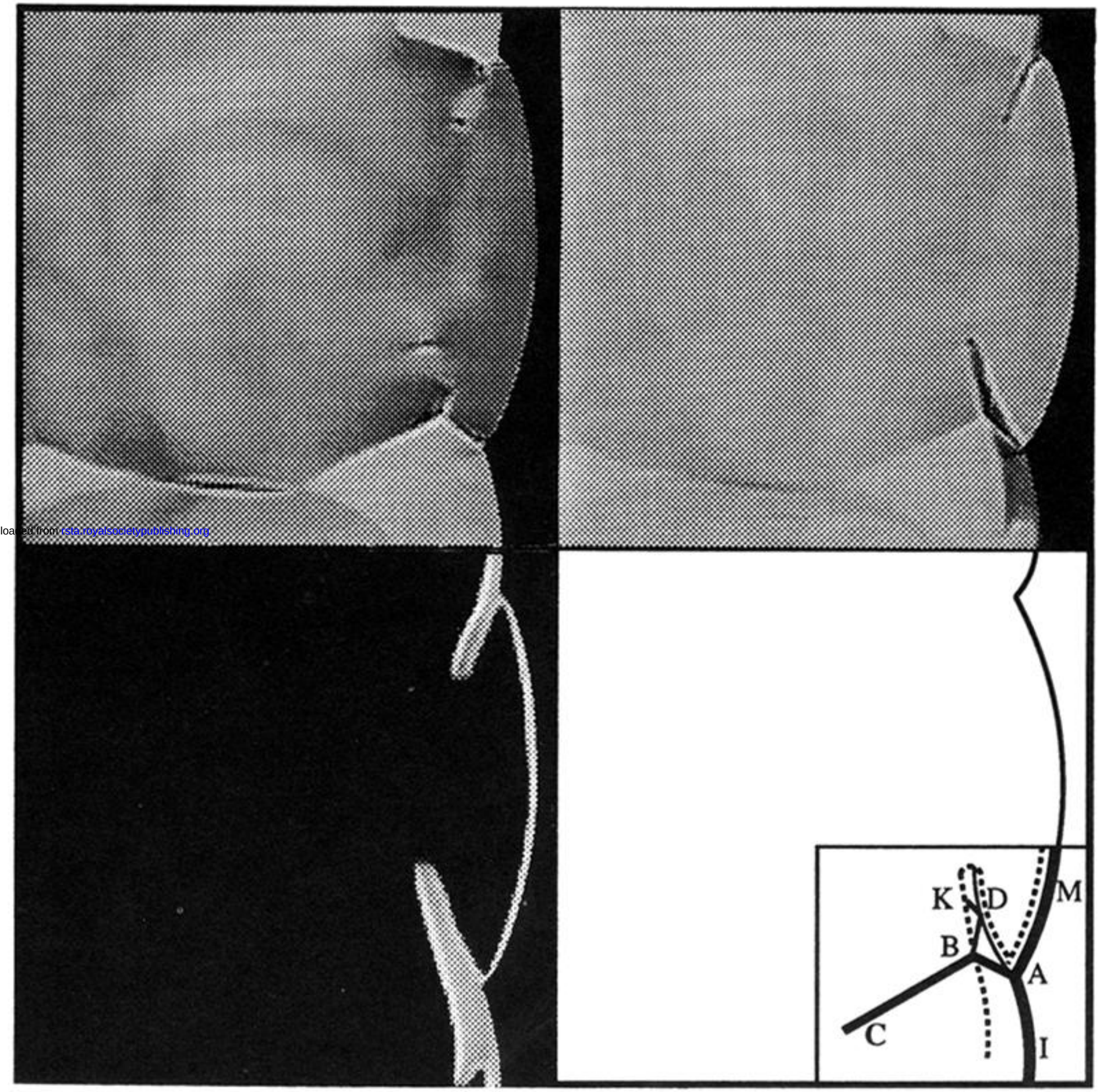

Figure 14. Snapshots of pressure (top left), density (top right), reactant mass fraction (bottom left) along with the corresponding wave diagram (bottom right). The detailed multiple Mach stem structure in the wake of the leading front is in surprising agreement with the experimental results of Voitsekhovskii *et al.* (1966). Following their notation, **M** is the Mach stem, **I** is the incident shock, **A** is the triple point, **AB** is the reflected shock, **B** is also the triple point for the secondary Mach stem configuration, **BC** is the transverse wave segment, **AD** is the slip line, **DK** is part of a centred rarefaction wave. Most of the reaction takes place between the leading shock and the dashed line.